Spring 5-2019

Solar Tracking Using a Parallel Manipulator Mechanism to Achieve Two-Axis Position Tracking

Joseph Otto Hubach
Rose-Hulman Institute of Technology, hubachjo@rose-hulman.edu

Solar Tracking Using a Parallel Manipulator Mechanism to Achieve Two-Axis Position Tracking

A Thesis

Submitted to the Faculty

of

Rose-Hulman Institute of Technology

by

Joseph Otto Hubach

In Partial Fulfillment of the Requirements for the Degree

of

Master of Science in Mechanical Engineering

May 2019

ROSE-HULMAN INSTITUTE OF TECHNOLOGY

Final Examination Report

Joseph Hubach — Name

Mechanical Engineering — Graduate Major

Thesis Title: Solar Tracking Using a Parallel Manipulator Mechanism to Achieve Two-Axis Position Tracking

DATE OF EXAM: February 13, 2019

EXAMINATION COMMITTEE:

	Thesis Advisory Committee	Department
Thesis Advisor:	Richard Stamper	ME
	Thomas Adams	ME
	Thomas James	EMGT

PASSED X **FAILED**

ABSTRACT

Joseph Otto Hubach

M.S.M.E.

Rose-Hulman Institute of Technology

May 2019

Solar Tracking Using a Parallel Manipulator Mechanism to Achieve Two-Axis Position Tracking

Thesis Advisor: Dr. Richard Stamper

A novel solar tracker is presented that uses a parallel manipulator for the tracking mechanism instead of a traditional serial manipulator. The motivation is to create a solar tracker that displays the advantages of two-axis tracking systems (e.g., increased exposure to incident radiation, and enabling the use of efficient concentrating solar cells) while addressing some of the disadvantages of current two-axis tracking systems (e.g., the difficulties associated with having actuators mounted to moving elements within the mechanism). The mobility of the proposed parallel manipulator is examined using Grübler's Criterion to establish that the manipulator displays the required two degrees of freedom. Additionally, a system of equations is developed for the proposed tracker that can be used for the forward or inverse kinematics analysis. Finally, the workspace of the proposed parallel manipulator-based solar tracker is presented.

DEDICATION

I would like to dedicate this thesis to my family who taught me the value of hard work and perseverance. I would not be in the position I am today without my mother, who taught me throughout grade school; my father, who supported me throughout life; my grandparents, who gave me wisdom throughout my life and put me to work early fixing their house; my brothers and sister, who pushed me to be my best self.

ACKNOWLEDGEMENTS

I would like to acknowledge everyone who helped and supported me throughout my work on this thesis. I would like to thank my advisor, Dr. Richard Stamper, for all his help. I would like to thank Dr. Constans for his help in developing the math model for the parallel manipulator. I would like to thank the faculty and my fellow students at Rose-Hulman for their help throughout my time at Rose-Hulman. Finally, I would like to thank my family for their support.

TABLE OF CONTENTS

Contents

LIST OF FIGURES

Figure Page

LIST OF TABLES

Table Page

LIST OF ABBREVIATIONS

2-PUU/RS	Two-Prismatic Universal Universal/Revolute Spherical
kWh	kilowatt-hour
GW	Gigawatt

LIST OF SYMBOLS

English symbols

l	The length of linkages in the manipulator
U	The universal joint type in the manipulator
P	The prismatic joint type in the manipulator
R	The revolute joint type in the manipulator
S	The spherical joint type in the manipulator
P_i	The displacement joint variable for the prismatic joint i

Greek Symbols

α	Elevation Angle
γ	Surface Azimuth Angle
γ_s	Solar Azimuth Angle
θ	A variable for various manipulator joint angles
ϕ	A variable for various manipulator joint angles
β	A variable for manipulator joint angles
φ	Angles that describe the orientation of the solar panel

1. INTRODUCTION

Over the past decade, solar power generation has become an increasingly popular form of electrical energy production. In 2017, nearly 100 GW of new photovoltaic systems were installed globally, and the cost of solar energy reached levels of just under 3 cents per kWh for some major installations [1]. This increased popularity can be attributed to many things, including the recent reductions in the cost of producing solar panels, the clean nature of solar power generation, increases in solar cell efficiencies, increases in battery storage capacity, government incentives, and the creation of better solar tracking systems.

While the production of solar energy has increased recently, there is still a great deal of potential for solar power to meet more of the world's energy needs. According to the International Energy Agency, only about 8% of the energy produced in 2016 was done so by renewable energies [2].

There are a few key ways to further improve the technology of solar power generation and distribution to make it an even more attractive method for producing electrical energy. The first technique is to create more efficient solar cells. The technology of solar photovoltaic cells continues to evolve and improve. In 2014, a French-German cooperation created a multi-junction concentrating solar cell with a 46% efficiency conversion rate [3]. To put that in perspective, in 2018, the typical solar installation used

crystalline silicon photovoltaic cells that have a conversion rate of 15% to 17% and reaches as high as 22.5% according to an article on Energysage [4]. The National Renewable Energy Laboratory has a useful chart that shows the various solar cells being developed and their efficiencies as shown in *Figure 1.1* [5]. A second method is creating batteries with higher storage capacity to service the market during hours when little to no electricity is being produced such as the nighttime or cloudy days. This is a vital aspect of solar technology which could lead to broader adoption of solar energy generation. A third way to improve solar energy production, and the one this thesis will focus on, is to improve the tracking mechanisms that are used to support and orient the solar panels. Aside from simply collecting more radiation, two-axis solar trackers also enable the use of advanced high-efficiency multi-junction concentrating solar cells that require accurate two-axis tracking to function properly.

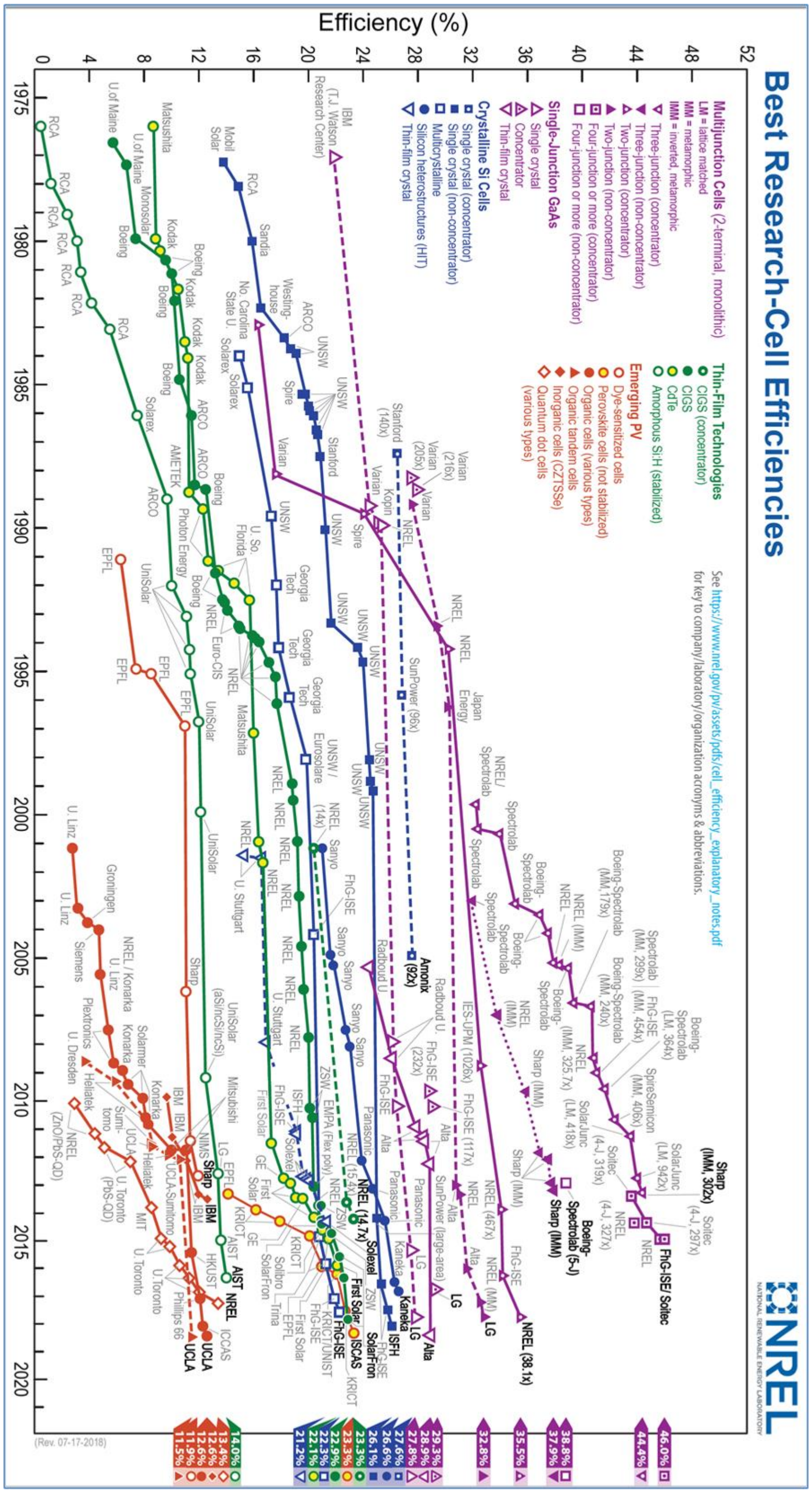

Figure 1.1: Solar cell efficiencies by National Renewable Energy Laboratory [5]

To increase the output of fixed solar panel installations, methods to track the sun and increase the exposure of the solar panel to direct sunlight have been developed. This technology is commonly referred to as solar tracking. A solar tracker for a photovoltaic panel is a frame that allows the photovoltaic panel to change orientations so that the solar panel follows the sun as the azimuth (γ_s) and elevation angles (α) of the sun change as shown in *Figure 1.2.* The goal of a flat panel photovoltaic tracking system is to minimize the angle of incidence (i.e, the angle formed by the sunbeam and normal of the panel) between the direct sunlight and the panel. The panel consequently tracks the sun to increase the amount of energy produced when compared to a fixed flat panel photovoltaic device.

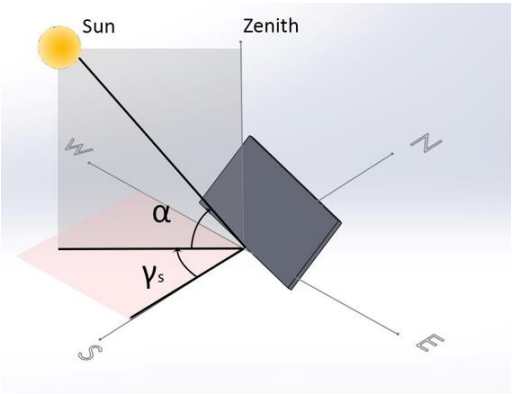

Figure 1.2: A representation of solar tracking angles, solar azimuth (γ_s) and elevation (α)

2. BACKGROUND

2.1 History of solar trackers

The first mechanical solar tracker was made in 1962 by Finster [6]. Later more solar trackers began to appear in the 1970s when several patents were issued for new devices that would track the sun in various ways. Among those patents is Amiztur Barak's US Patent 3,982,526, which was assigned to the United States Energy Research and Development Administration's [7]. Barak's device, *Figure 2.1*, is a solar panel frame with two heat expansive elements and a shaded plate all on a polar axis oriented toward the sun to track it throughout the day. In the morning, the first heat expansive element would heat the thermal expansion fluid and orient the solar panel toward the sun while the second heat expansive element was shaded by the plate. Throughout the day, the second heat expansive element would then heat the thermal expansion fluid as the sun moved and orient the solar panel toward the sun again while the first heat expansive element is shaded. This device was innovative due to its lack of need for power to move the device and it increased the output of a solar panel beyond the fixed panel; however, it did suffer some problems. The number of positions was limited to two, the amount of time to heat initially would vary around an hour, and the fluid would need maintenance over time due to leaking. Also, the system falls short on cloudy days or colder weather which does not allow it to heat up as effectively.

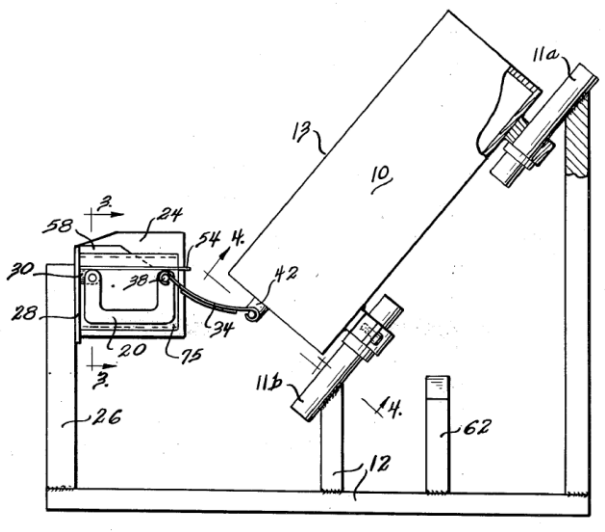

Figure 2.1: The passive solar tracker from US Patent No. 3,982,526

Another patent of interest was US Patent 4,011,854 that was assigned to the National Aeronautics and Space Administration by Lott Brantley and Billy Lawson [8]. Brantley and Lawson's device, *Figure 2.2*, was a rigid, angulated axle with a straight midportion to support a collector dish and opposite end portions supported by spaced journals. The two opposite end portions have a drive to move the collector for seasonal changes while the two spaced journals were driven to account for daily changes. This innovative device allowed for continuous tracking of the sun not only throughout the day but also accounting for the seasonal rotation of the earth. Despite its innovative approach and continuous tracking abilities, the device is still limited in its movements and does not achieve the full range of tracking.

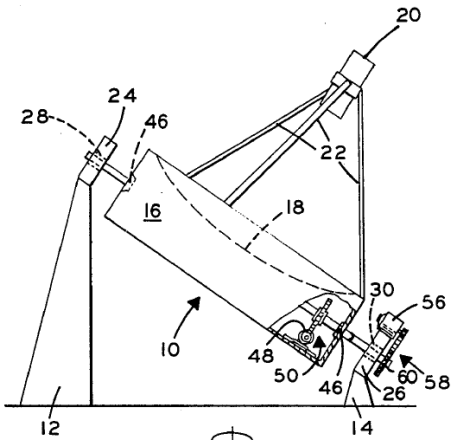

Figure 2.2: The two-axis tracker from US Patent No. 4,011,854

Moving beyond the first solar trackers, many inventors started building on the idea. Through time, a common method to increase the solar panel output became the single-axis trackers. Single-axis trackers can move one degree of freedom in horizontal, vertical, tilted, or polar aligned directions as shown in *Figure 2.3*, to track the sun throughout the day. When compared to a fixed solar mount, single-axis trackers such as Gay's can increase the output of a solar panel by approximately 30% [9]. Two-axis trackers, on the other hand, have two degrees of freedom and can move in two directions that are generally normal to each other. A common two-axis tracker configuration is the azimuth-altitude tracker, see *Figure 2.3*. The two-axis changes allow them to not only track the sun throughout the day but also through the seasons as the sun changes its position relative to the earth due to the rotation of the earth. A two-axis tracker can follow the sun throughout the year. According to Muhammad and Karim in their paper on hybrid automatic solar-tracking systems design, an increase of 18% over single-axis trackers can be attained using a two-axis tracker in some circumstances [10].

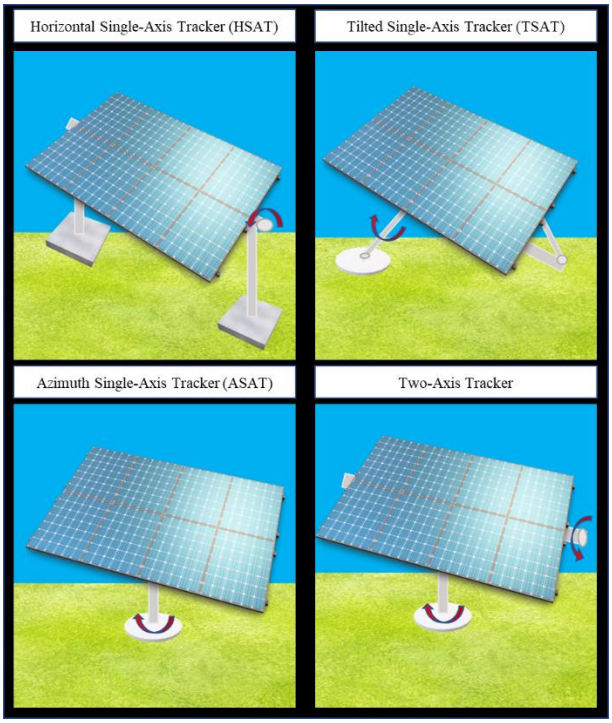

Figure 2.3: A diagram of single-axis tracker and two-axis tracker types

Another classification scheme divides solar trackers into categories of continuous tracking systems or discrete tracking systems. Continuous trackers are systems that continuously track the sun through the entire day using sensors or controls systems that constantly adjust the solar panels. In contrast, discrete trackers move through some number of predetermined discrete positions throughout the day. Discrete trackers attempt to reduce cost and complexity by focusing on just a few positions thus allowing for simpler control systems and less expensive actuators.

Many of the large companies that design and fabricate commercial trackers (e.g., NEXTracker, Array Technologies, and Soltec) concentrate on continuous single-axis trackers. This can primarily be attributed to the attractive ratio of cost relative to performance that single-axis trackers currently enjoy. Even though continuous two-axis

trackers can increase the output compared to a single-axis tracker by as much as 18%, the additional initial capital costs and ongoing maintenance expenses of the two-axis tracking systems make them unattractive.

2.2 Current technology – single-axis trackers

Continuous single-axis trackers have become the most common tracker due to their ability to significantly increase the output of a solar panel while being less expensive than conventional two-axis trackers. Also, many panels can be oriented by a single mechanism since they can be arranged so that a long row of panels can be driven by a single shaft. One of the leaders in solar tracking technology that takes advantage of this is Array Technologies. Array Technologies boast a horizontal single-axis tracker called the DuraTrack HZ v3. This tracker utilizes a frame that interconnects each solar panel in a given row to a torque tube that is supported every few feet. Additionally, multiple gearboxes connect each torque tube to a single central drive shaft. The entire assembly is driven by a single motor. This device is patented through US Patent No. 8,459,249 and US Patent No. 9,631,840 [11][12]. These patents disclose the device and the method to drive a collection of solar panels with a single motor as shown in *Figure 2.4.* Array Technologies is an industry leader due to their robust technology that requires minimal maintenance. This creates an attractive package that provides an increased output over fixed panels.

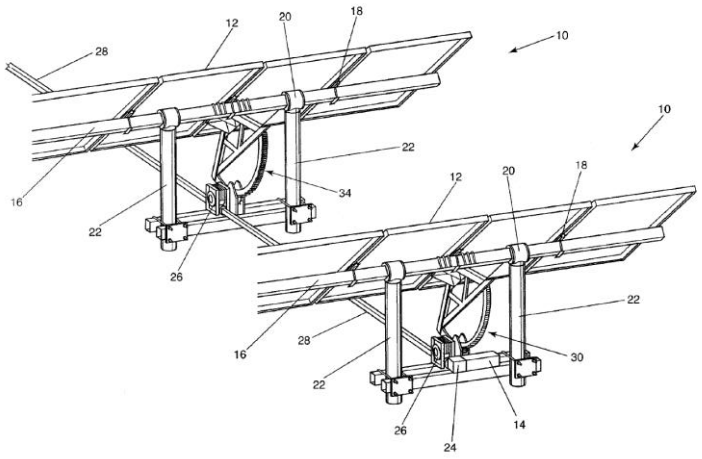

Figure 2.4: Array Technologies single-axis tracker in US Patent No. 8,459,249

NEXTracker is another industry leader in solar tracking with its NX Horizon solar tracker shown in *Figure 2.5*. The NX Horizon is a self-powered horizontal single-axis mass balanced tracker. This device has many patents including US Patent No. 9,543,888, US Patent No. 9,905,717, and US Patent No. 10,075,125 [13][14][15]. The NX Horizon is made up of torque tubes with an adjustable hanger assembly and clamshell clamps assembly, shown in *Figure 2.5*, to attach the solar panels and ends of the torque tubes. The center of mass is aligned with the center of cylindrical torque tubes to create a mass balanced solar tracker that reduces torque on the motor. This tracker, unlike the DuraTrack HZ v3, does not connect in-between rows. Each row is its own assembly. The patents also assert that it is frameless which allows the modules to sit closely together and thus waste less space.

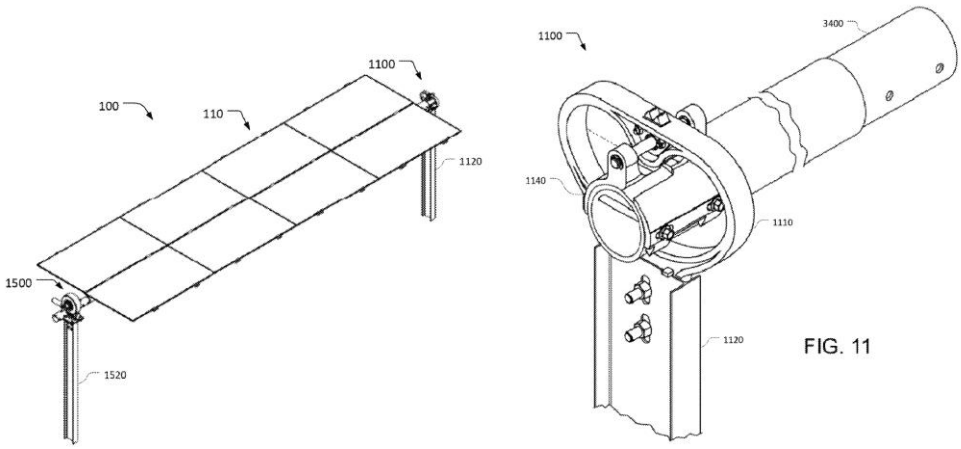

Figure 2.5: The NEXTracker's single-axis tracker from US Patent No. 10,075,125

One company that makes tilted single-axis solar trackers that moves away from the traditional single-axis solar tracker is SunPower. SunPower has a US Patent No. 8,776,781 on the T20 Tracker [16]. The T20 Tracker is a single-axis tilted solar tracker that includes a tube that is rotatable on an end-to-end axis. The first support at the lower end has a translation mechanism that is coupled with tube and connected to a base. The second support is connected to a V-frame or A-frame which is then supported by two bases at the end of the frame. This tilted design allows the sun to be tracked in a way that is different from other single-axis trackers. *Figure 2.6* shows that the solar tracker has a pre-determined fixed tilt and the device uses a gear system at the lower end to turn the torque tube to track the sun in a single-axis.

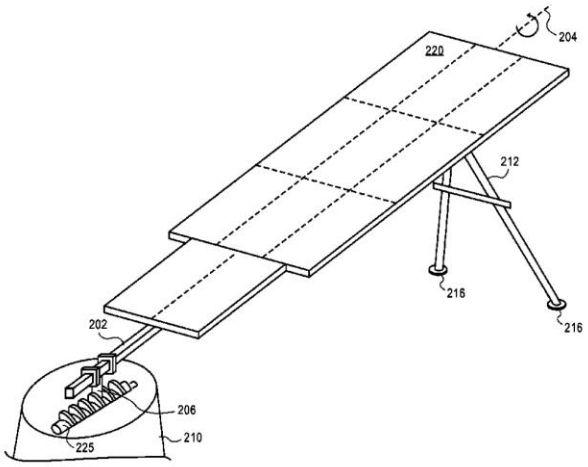

Figure 2.6: SunPower T20 solar tracker mechanism

An innovative approach to solar tracking is the kirigami method proposed by Lamoureux et al [17]. Kirigami has origins in Japan and is the art of cutting paper. Lamoureux had the idea to take thin-film gallium arsenide solar cells and cut patterns into them to create a lightweight solar tracker without the use of costly and cumbersome structural components. The solar cells can move and track the sun through strain put in the axial direction perpendicular to cuts as shown in *Figure 2.7*. The strain creates a controlled buckling parallel to the cuts in the traverse direction and a change in the angle that is synchronized along its length. The solar cells can also tilt clockwise by lifting or lowering one end of the sheet before applying strain. The solar cell sheets would be housed in a double pane enclosure for weatherproofing.

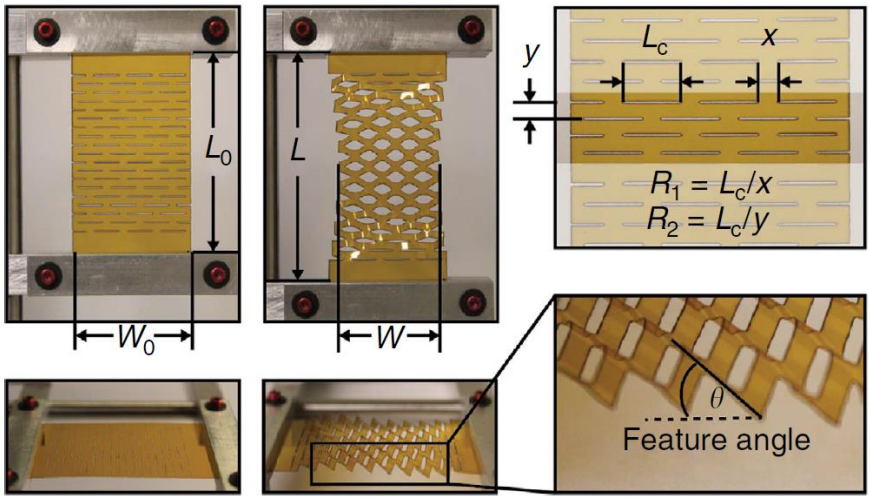

Figure 2.7: Kirigami solar tracker demonstration of concept [17]

Another way to reduce the cost of solar tracking presented by Huang and Sun is to create a single-axis three position discrete solar tracker [18]. The tracker, shown in *Figure 2.8*, moves only three times a day to increase the output when compared to a fixed solar panel, but also decrease the power consumption and controls complexity compared to a continuous tracker. The goal is to capture some, if not all, of the increased power generation of a solar tracker which according to Huang, is 41% for a two-axis and 36% for a single-axis tracker when compared to a fixed panel (this difference in the estimated increase in solar power generation for solar trackers over fixed trackers can be attributed to factors such as the solar cells used, the location, and the climate the solar panel resides in). The idea is to have the solar panel stop at three angles using a touch switch mounted on a transmission gear of the frame. The three angles are pre-cut into the touch switch which allows the mechanism to stop until it's given the signal at the time of day to move again. According to Huang, this resulted in a 23% power generation gain and price reduction of around 20% to 30%.

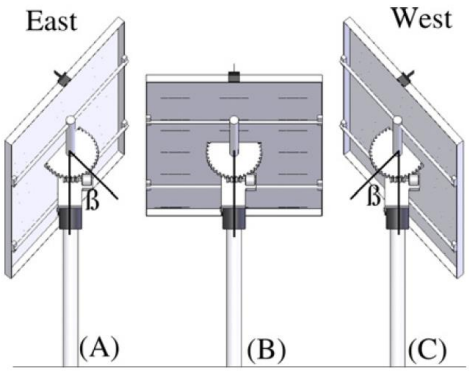

Figure 2.8: The 3-position discrete tracker [18]

2.3 Current technology – two-axis trackers

Two-axis trackers are generally more sophisticated than single-axis trackers because not only do they require more components and actuators, but their controls, software, and sensors are more complex. The general two-axis tracker operates by using an axis to move the solar panel in the azimuth direction and another axis in the altitude direction. A simple representation of this motion can be seen in *Figure 2.9*. The azimuth direction is tracking the sun left to right as the vertical axis of rotation is moving in *Figure 2.9*, whereas the altitude axis tracks the sun up and down as demonstrated by the diagonal axis of rotation in *Figure 2.9*.

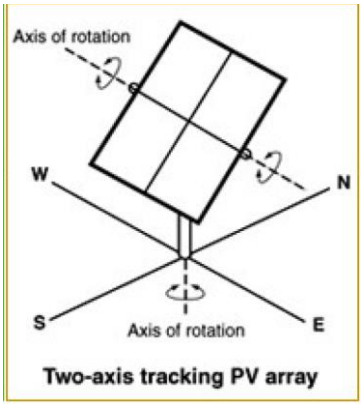

Figure 2.9: Two-axis tracker representation

An example of a two-axis tracker is in *Figure 2.10*, Suncore Photovoltaics' US Patent No. 8,946,608 [19]. The two-axis tracker is powered by two motors that control axes with respect to the sun. The first motor controls the inclination angle, or altitude angle, relative to the ground. The second motor is used to rotate the solar panel about an axis perpendicular to the surface created by the second axis or rotate the azimuth angle. The solar tracker also includes an algorithm to predict the future location of the sun and a computer model to determine the position the motors need to move to align substantially with the sun at a future time.

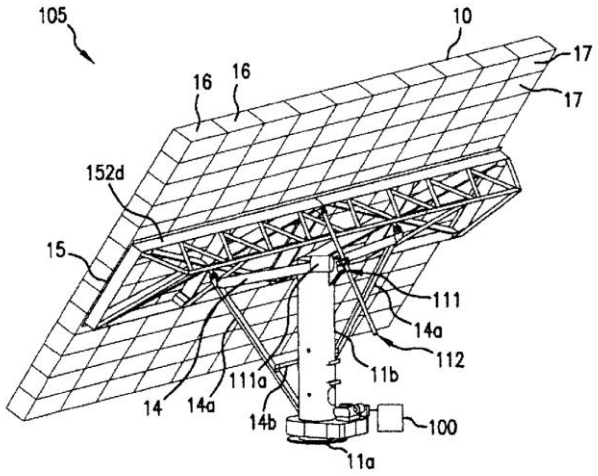

Figure 2.10: Suncore Photovoltaics' two-axis tracker from US Patent No. 8,946,608

Another approach to two-axis tracking can be seen in US Patent No. 8,895,836 by Amin et al [20]. *Figure 2.11* shows the frame of the design, which incorporates an azimuth actuator to adjust the azimuth and an elevation actuator to adjust the elevation of the panel seat. The panel seat is a method to hold the solar panel with a rotating arm and two pins to connect the solar panel. A support, labeled 505 in *Figure 2.11*, is positioned

to hold the panel seat up and serve as an elevation pivot. The device does not use any sensors and instead relies on a controller that uses latitude, longitude, time of day, and date to adjust the solar panel seat to track the sun.

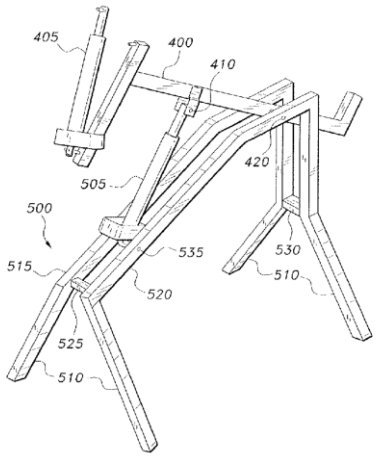

Figure 2.11: A two-axis tracker frame from US Patent No. 8,895,836

An innovative two-axis tracker is introduced by Jeng et al to simplify the two-axis tracker [21]. Jeng et al designed a spatial parallel manipulator two-axis tracker to allow for increased motion, but also increase the rigidity of the frame. Jeng accomplishes this with the use of dual-glide manipulators that are actuated by servomotors. These glides serve as prismatic joints and a central supporting pole is utilized to pivot and move the solar panel as seen in *Figure 2.12***.**

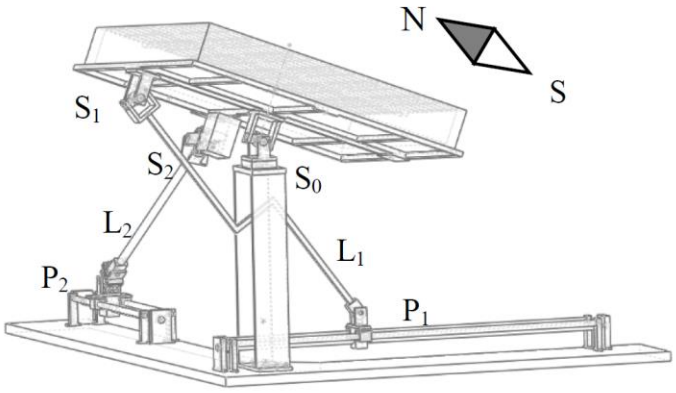

Figure 2.12: A two-axis spatial parallel manipulator solar tracker [21]

The prismatic joints use a universal joint and a revolute joint to connect to the limbs. The limbs and central pivot use spherical joints to connect to the solar panel. A second configuration is also created by utilizing a second universal joint in the place of the revolute joint. This creates a device with 2 degrees of freedom according to Jeng. No efficiency is reported by the paper, but Jeng claims that the device is much faster than the traditional two-axis tracker and provides more accuracy.

SolarCity Corporation introduced another alternative approach in US Patent No. 9,494,341 [22]. The solar tracker is a discrete mechanism that is controlled by a fleet of robots that run on tracks and use a modular tool to adjust the solar panels as depicted in *Figure 2.13*. The system is optimized so that the robots will move according to a task organizer or central intelligent control to optimize battery life and movements. This allows the solar panels to be adjustable without having their own actuators to in theory reduce the cost.

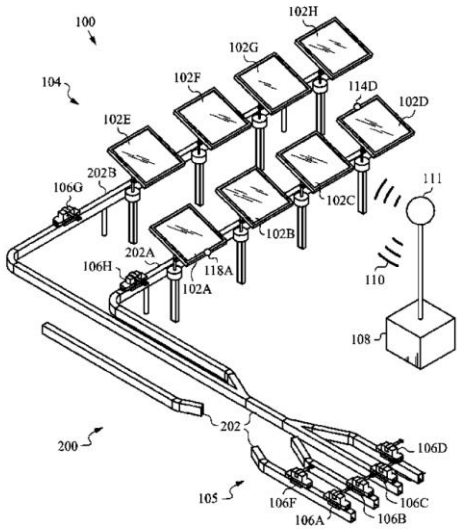

Figure 2.13: SolarCity Robot Discrete Tracking System from US Patent No. 9,494,341

2.4 Summary

Despite the impressive technology available today for solar tracking, there is still room for improvement. An obvious drawback for single-axis trackers is the ability to only move in one direction. This means that as the seasons change the tracker is losing potential sun as it becomes more misaligned. This becomes even more rampant the further one moves away from the equator, northward or southward due to the higher variance of the solar angle between the summer and winter seasons. Numerous companies produce the single-axis tracker which is a row of solar panels interconnected by a torque tube in which the solar panels will rotate to track the sun in one degree of freedom. Although this might be the most attractive and cost-effective method at the moment, it leaves room for improvement until two-axis tracking can compete. However, current two-axis trackers, with the exception of Jeng's, are still based on serial kinematic configurations that require actuators be mounted to moving linkages and large structural

elements to overcome the lack of rigidity that is inherent to serial structures. So there is still an opportunity to improve the state of the art for two-axis trackers

3. MOTIVATION

The motivation for the work presented in this thesis is to develop a novel solar tracking mechanism that provides the advantages of two-axis tracking systems (e.g., increased exposure to incident radiation, and enabling the use of efficient concentrating solar cells) while having the potential to mitigate the disadvantages of current two-axis tracking systems (e.g., the need to use heavy and expensive structural elements to compensate for the lack of rigidity inherent to serial manipulators, and the difficulties associated with having actuators mounted to moving elements within the mechanism).

Today, nearly all two-axis solar tracking mechanisms commercially sold are serial manipulators. A serial manipulator is a term used to describe an actuated mechanism that is comprised of a combination of links and joints arranged serially. A traditional industrial robot arm is an example of a serial manipulator. Serial manipulators form a single open kinematic chain in which the end effector can be moved in open space to achieve the desired motions or positions. *Figure 3.1* shows a group of solar panels that use traditional serial manipulator mechanism to achieve two-axis tracking. These are two-axis trackers installed at the Sheridan Community Schools north of Indianapolis. Two-axis trackers were used in this installation since the school corporation had a limited footprint for the solar installation, and they needed to increase the output for the given footprint. Had more land been available, they would have used fixed panels.

Figure 3.1: An installation of two-axis solar trackers at the Sheridan Community School

The two-axis tracker serial mechanism from the Sheridan Community School can be seen more closely in *Figure 3.2*. As *Figure 3.2* shows, the traditional two-axis tracker utilizes a rotating base to vary the azimuth angle, and a torque tube to vary altitude angle to change the solar panel's position. The actuator used to vary the altitude angle and rotate the torque tube needs to be directly mounted to the rotating base. This rotating base member needs to be a large structural tube for stiffness as *Figure 3.2* shows. If the two-axis tracker supported the panels with multiple legs, the amount of material needed to support the panel and resist the loads acting on the solar panel could likely be reduced.

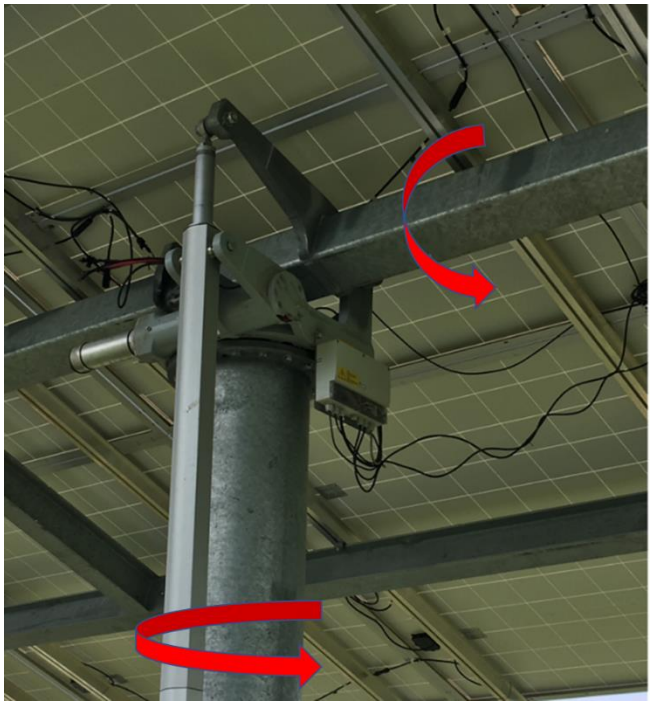

Figure 3.2: Two-axis tracker serial manipulator close-up

Trackers that use parallel manipulators as the tracking mechanism provide an alternative to serial manipulator trackers. Parallel manipulators are mechanisms composed of two or more closed kinematics chains to support a mobile platform. The number of actuators associated with a parallel manipulator typically equals the number of degrees of freedom. One of the advantages of parallel manipulators is that these actuators can be mounted on or near the base. The number of degrees of freedom for a manipulator is determined by the number and configuration of links, joints, and joint movements. This provides an advantage for parallel mechanism since the moving structure doesn't need to support the weight and inertial effects of the actuators. An example of a parallel manipulator is the mechanism found under 6 degree-of-freedom flight simulators where there are six actuators positioned under the mockup of the cockpit. A serial manipulator

that would achieve the same function for a flight simulator would need to be a much more massive device than the analogous parallel manipulator.

Some reasons that a serial manipulator is used over a parallel manipulator is that in theory, they are much simpler. The mathematics behind serial manipulators is less complex. Additionally, serial manipulators generally display a larger workspace for a comparably sized mechanism. They are easy to demonstrate and model since they use simple motions such as rotating about an axis. And finally, they are also more well-known and have been used in practice for much longer.

However, the less common alternative, parallel manipulators, may be the key to creating a better solar tracker. There are many advantages that parallel manipulators have. In general, parallel manipulators have high accuracy, rigidity, speed, and load capacities [23]. One of the problems with current solar trackers is the large load which leads to large support structures being required for trackers based on serial mechanisms. In turn, these large support structures require more material which drives up the cost. Parallel manipulators by nature have more rigidity and load carrying capacity due to their distributed load over the kinematic chains and actuators being mounted at the base. The high accuracy of parallel manipulators also reduces errors that are accumulated by serial chains. This could allow less complex controllers and less precise actuators to move the mechanism. Parallel manipulators are also becoming more prevalent in other industries despite the more complex kinematics and small workspace. For example, parallel

manipulators such as the three degrees of freedom delta robot are increasingly being used as pick and place robots where high-speed accurate operation is required.

4. DESCRIPTION OF THE PROPOSED TRACKING SYSTEM

4.1 Sun position vector

The position of the sun can be described using an azimuth angle, γ, and elevation angle, α, which is shown in *Figure 4.1* with respect to a reference Cartesian coordinate system.

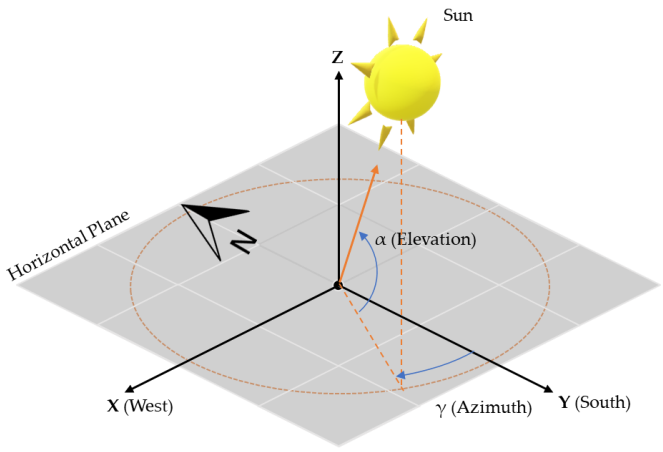

Figure 4.1: The sun reference coordinate system

For the tracking system, the *Y*-axis points toward the south; the *X*-axis points westward; the *Z*-axis points upward normal to the surface of the earth which is represented as the horizontal plane. The horizontal plane is created by the *XY*-plane and is tangent to the surface of the earth. The azimuth angle, γ, is a polar angle in the horizontal plane. The azimuth angle is defined relative to the south and is measured positive to the west and negative to the east. The elevation angle, α, is measured from the same horizontal plane, where positive is above the horizontal plane and negative is below the horizontal plane. *Equation 4.1* is a unit vector which points toward the sun and is in terms of the reference coordinate system.

$$\boldsymbol{n} = [\cos\alpha\sin\gamma \quad \cos\alpha\cos\gamma \quad \sin\alpha]^T \tag{4.1}$$

4.2 Two-axis parallel manipulator tracker

The proposed mechanism for two-axis tracking is a parallel manipulator with one spherical joint, one revolute joint, two prismatic joints, and four universal joints. A schematic representation of this parallel manipulator is displayed in *Figure 4.2*.

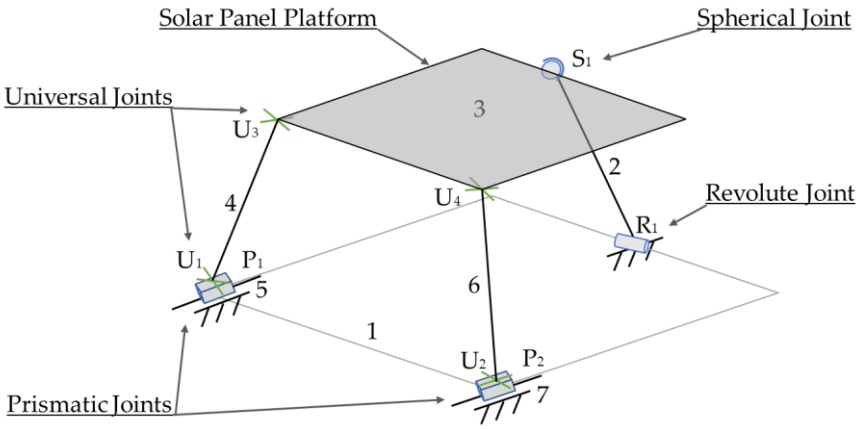

Figure 4.2: A schematic representation of the 2-PUU/RS parallel manipulator tracking mechanism

The mechanism is made up of a base platform or ground, numbered link 1 in the schematic. This base platform is then connected to 3 legs or kinematic chains. One of the chains is made up of a prismatic joint, P_1, connected to the ground, link 1. The prismatic joint, P_1, is then connected to a universal joint, U_1, via link 5. The universal joint, U_1, is then further connected to another link 4 which serves as an intermediate member to another universal joint, U_3. The universal joint, U_3, then connects to a mobile platform, link 3. A second symmetrical kinematic chain is created with identical components

(comprising of link 1, P_2, link 7, U_2, link 6, U_4, link 3). A third and final kinematic chain uses a revolute joint, R_1, that is connected to the base, link 1. This revolute joint, R_1, uses an intermediate link, link 2, to connect to a spherical joint, S_1, which is also connected to the mobile platform, link 3. The mobile platform, link 3, is where the solar panel will rest. This can be called a 2-PUU/RS parallel manipulator mechanism for short. The inputs of the system are the displacement of the two prismatic joints, joint P_1 and joint P_2. The movement of the two joints creates an output of the desired orientation of the mobile platform, link 3. This orientation will be directed toward the sun for more effective energy production.

An alternative depiction of the parallel manipulator is displayed in *Figure 4.3*. This serves as an illustration of the mechanism in graph representation.

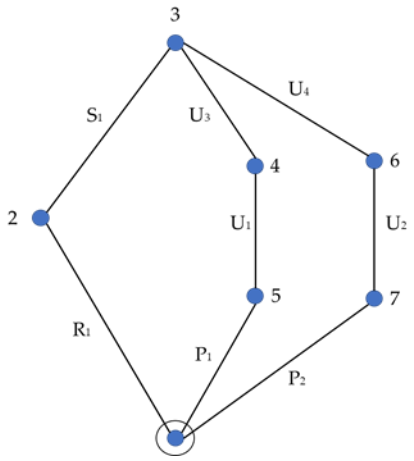

Figure 4.3: Graph representation of the 2-PUU/RS parallel manipulator tracking mechanism

Graph representation is an abstraction that uses vertices as links and edges/lines as joints. The edge connections correspond to pair connections between links. The edge connections can be either labeled or colored in various ways to distinguish the different

joint types. Finally, a mechanism with a fixed link can be denoted using two concentric circles [24]. The importance of these graph representations is that it can facilitate enumeration of other similar mechanism and does not conform to just one configuration. However, in *Figure 4.3*, the graph representation does use the same notation to label each joint and link to allow connection to the two schematics to be made.

A SolidWorks model of the parallel manipulator solar tracker was created. In *Figure 4.4*, the tracker is seen with the two PUU chains in identical positions with the cylinder fully retracted. The prismatic joints, when fully retracted, will be defined as position 1. Position 2 is when the prismatic joint is at the end of the slider track. The tracker will display at least three different configurations of these positions that create an ideal angle of incidence for the sun at various times during the day. *Figure 4.5* shows the device in the extreme position where the left PUU kinematic chain is in position 2 and displaced from the actuator whereas the right one remains in position 1. Finally, *Figure 4.6* shows the device with the opposite configuration where the right PUU kinematic chain is in the displaced position 2.

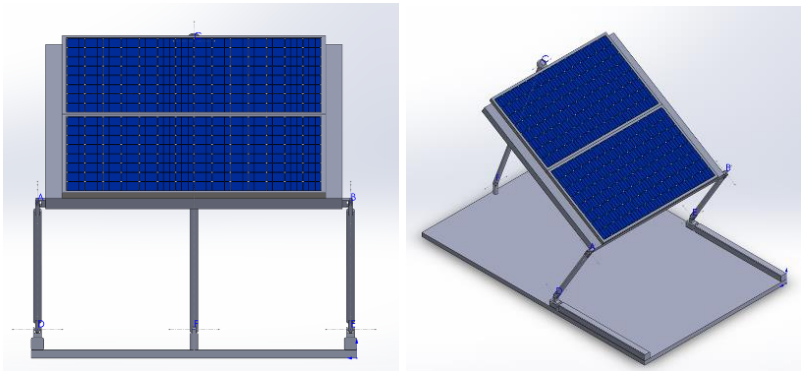

Figure 4.4: The solar tracking parallel manipulator in an example position that orients the solar panel to $\gamma = 0^{o}$ and $\alpha = 58.7^{o}$

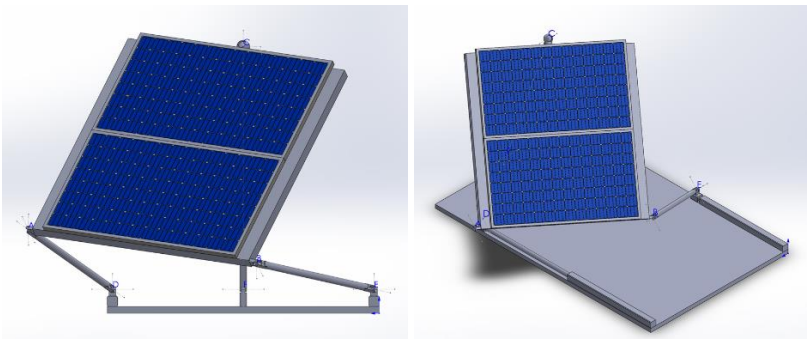

Figure 4.5: The solar tracking parallel manipulator in an example position that orients the solar panel to $\gamma = 22.4^{o}$ and $\alpha = 38.8^{o}$

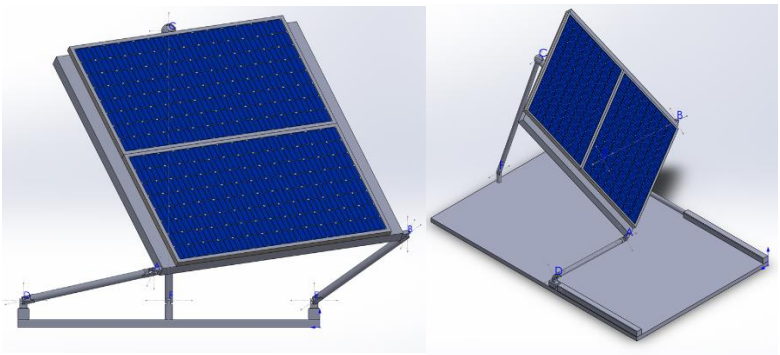

Figure 4.6: The solar tracking parallel manipulator in an example position that orients the solar panel to $\gamma = -22.4^{o}$ and $\alpha = 38.8^{o}$

4.3 Mobility analysis

The proposed device, a 2-PUU/RS parallel manipulator, is intended to track the sun in two axes. In order to move in two axes, the device must have two degrees of freedom. Therefore, it must be demonstrated that this device does have just two degrees of freedom. The 2-PUU/RS parallel manipulator means it has two symmetric links each with its own prismatic joint and two universal joints and then another link with just a revolute joint and a spherical joint. The parallel manipulator mechanism degrees of freedom can be calculated using the *Grubler Mobility Equation***,** where F is the number of degrees of freedom the mechanism contains, and λ, or motion parameter, is the degrees of

freedom which the mechanism is intended to operate in (i.e. $\lambda = 3$ for planar and spherical mechanisms and $\lambda = 6$ for spatial mechanisms). The parameter n is the number of links in the mechanism, which includes fixed links. The parameter j is the number of joints in the mechanism. And finally, f_i is the relative motion permitted by joint i.

$$F = \lambda(n - j - 1) + \sum_{i=1}^{j}(f_i) \tag{4.2}$$

Table 4.1: Parallel Manipulator Mechanism Parameters

Mechanism Movement Parameters	
Spatial Movement, λ	6
Number of Link, n	7
Number of Joints, j	8
Number of 1 Degree of Freedom Joints	3
Number of 2 Degree of Freedom Joints	4
Number of 3 Degree of Freedom Joints	1

Using this information from *Table 4.1*, the number of degrees of freedom can be solved for using the *Grubler Mobility Equation*, which is presented as *Equation 4.2***.** The number of degrees of freedom for the parallel manipulator is F = 2. Therefore, this mechanism does, in fact, have two degrees of freedom.

4.4 The kinematics of the proposed 2-PUU/RS solar tracker

The kinematic analysis of the proposed tracker assumes that a fixed *XYZ* coordinate system is rigidly attached to the corner of the stationary base at point O, which is also where the non-displaced point E temporarily resides as shown in *Figure 4.7*. The *Z*-axis is normal to the base. The *Y*-axis aligns with the prismatic joints and faces south. The *X*-axis is in a common right-hand coordinate position with respect to *Z*-axis and *Y*-axis. Additionally, the moving reference frame *UVW* is attached to point B of the mobile

platform as shown in *Figure 4.7*. The *W*-axis is normal to the mobile platform. The *U*-axis is pointing toward point A along a line created by point A and B where the two universal joints reside. The *V*-axis is in the common right-hand coordinate position with respect to the *W*-axis and *U*-axis.

The kinematic analysis of the proposed general 2-PUU/RS manipulator is also limited to a special case of the general 2-PUU/RS. In particular, the following simplifying assumptions and constraints were made for the kinematic analysis: the axes of the prismatic joints are parallel to the *Y*-axis; the universal joints, U_1 and U_2, have a fixed yoke that is always parallel to the *X*-axis; the universal joints, U_3 and U_4, have a fixed yoke that is always parallel to the mobile platform's *W*-axis; the joints at points A, B, and C are all in the *UV*-plane; and the joints at points D, E, and F are all in the *XY*-plane.

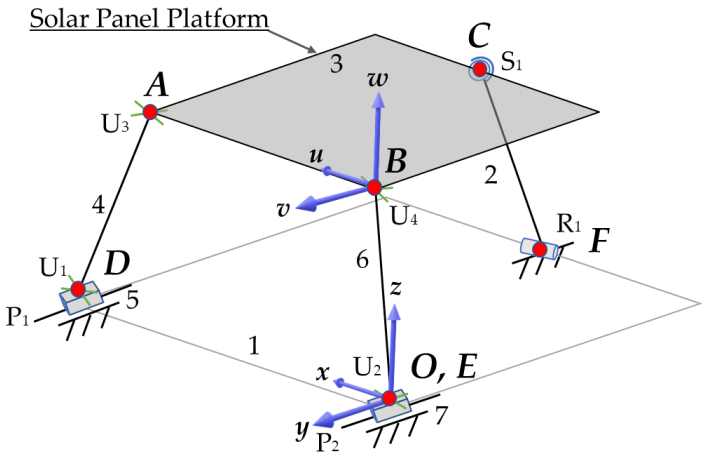

Figure 4.7: The Moving Frame *UVW* attached to the solar panel at Point C

The mobile platform of the 2-PUU/RS mechanism is supported by a spherical pivot at point C and two universal joints at point A and B. These supports allow two degrees of freedom of movement in order rotate to the desired azimuth and elevation angle to track the sun. The two universal joints are comprised of two U-shaped yokes which connect perpendicular to each other using a cross-shaped member in the middle of the two yokes. One yoke is mounted to the mobile platform and the other is mounted to a link that connects to another universal joint. These links are link legs 4 and 6. Following the connection of universal joints, a prismatic joint is connected to the universal joint to complete the chain to the ground.

The spherical joint at point C acts as a passive pivot because the two prismatic joints act as the driving mechanism for the mobile platform movement. The input of the two prismatic joints moves the connected universal joints and members to transition the mobile platform from one position to next. The movement of the prismatic joints transitions the mobile platform to different positions by rotating the mobile platform to the desired azimuth and elevation angles, which can be described by a series of rotations about the *W*-axis and the *U*-axis. The orientation of the moving platform can be described using a first rotation φ_1 about the *W*-axis, which is related to the azimuth angle. The rotation is displayed in *Figure 4.8*.

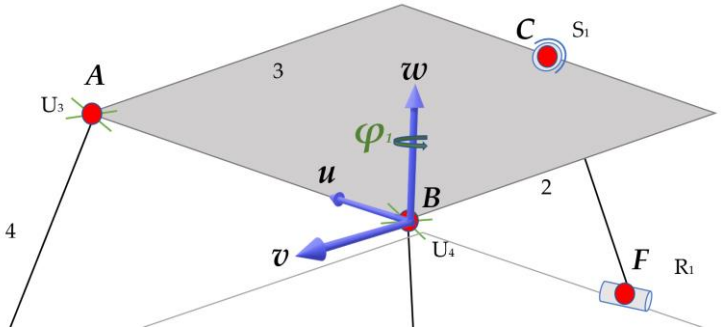

Figure 4.8: The Rotation about the *W*-axis of the moving reference frame (φ_1)

The moving *UVW* coordinate system can be described as *U'V'W'* after this first rotation. A second rotation φ_2 about the displaced *U*-axis (now in the *U'* position), which is related to the elevation angle. The rotation is visually shown in *Figure 4.9* for φ_2.

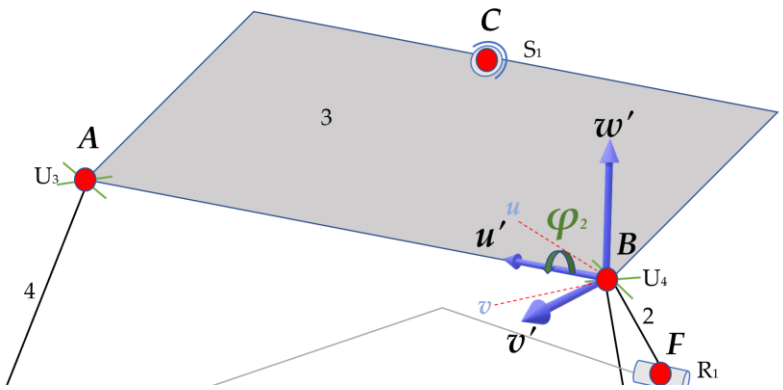

Figure 4.9: The Rotation about the *U*-axis of the moving reference frame (φ_2)

The moving *U'V'W'* coordinate system then becomes *U''V''W''*. Finally, a third rotation φ_3 about the displaced *W*-axis (now in the *W''* position). The rotation is visually shown in *Figure 4.10* for φ_3.

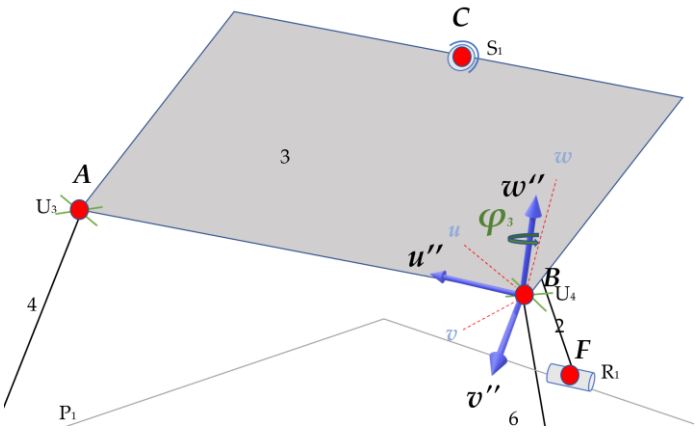

Figure 4.10: The rotation about the displaced *W*-axis of the moving reference frame (φ_3) [w represents the original *W*-axis position]

The orientation of the mobile platform can be expressed in terms of *XYZ* fixed reference frame using a 3x3 orthogonal matrix **R,** or *Equation 4.3*. The three unit vectors, $\boldsymbol{r_1}$, $\boldsymbol{r_2}$, and $\boldsymbol{r_3}$, are mutually orthogonal in the positive **u**, **v**, and **w**-directions, respectively. Any position vector in the moving reference frame *UVW* may be expressed in terms of $\boldsymbol{r_1}$, $\boldsymbol{r_2}$, and $\boldsymbol{r_3}$.

$$\boldsymbol{R}(\varphi_1, \varphi_2, \varphi_3) = [\boldsymbol{r_1} \;\; \boldsymbol{r_2} \;\; \boldsymbol{r_3}] \tag{4.3}$$

Where

$$\boldsymbol{r_1} = \begin{bmatrix} \cos\varphi_3\cos\varphi_1 - \sin\varphi_3\cos\varphi_2\sin\varphi_1 \\ \cos\varphi_3\sin\varphi_1 + \sin\varphi_3\cos\varphi_2\cos\varphi_1 \\ \sin\varphi_3\sin\varphi_2 \end{bmatrix}$$

$$\boldsymbol{r_2} = \begin{bmatrix} -\sin\varphi_3\cos\varphi_1 - \cos\varphi_3\cos\varphi_2\sin\varphi_1 \\ -\sin\varphi_3\sin\varphi_1 + \cos\varphi_3\cos\varphi_2\cos\varphi_1 \\ \cos\varphi_3\sin\varphi_2 \end{bmatrix}$$

$$\boldsymbol{r_3} = \begin{bmatrix} \sin\varphi_2\sin\varphi_1 \\ -\sin\varphi_2\cos\varphi_1 \\ \cos\varphi_2 \end{bmatrix}$$

One way to think about these vectors is exemplified by the relationship between $\boldsymbol{r_1}$ and **u**. The vector $\boldsymbol{r_1}$ is the same unit vector as **u**, but $\boldsymbol{r_1}$ is expressed in terms of the fixed *XYZ* coordinate system where u is expressed in terms of the *UVW* moving coordinate system.

Using the azimuth angle, γ, and elevation angle, α, of the sun, the two angles of rotation of the moving platform that are required to set the orientation of the solar panel platform can be calculated.

$$\varphi_1 = -\gamma \tag{4.4}$$

$$\varphi_2 = (\alpha - 90) \tag{4.5}$$

Equation 4.4 simply uses the negative azimuth angle of the sun to rotate about the *W*-axis of the mobile platform. *Equation 4.5* using the elevation angle minus 90 degrees for a rotation about the displaced *U*-axis to achieve the desired slope of the mobile platform. The third rotation angle φ_3 becomes an unknown that will need to be determined in conjunction with the other parameters. This third rotation is the rotation of the solar panel about the axis normal to the solar panel and has no impact on the performance of the solar panel.

In order to do the kinematic analysis, a moving coordinate system is also defined for each of the joints at B, D, and E. The axes of the moving coordinate systems are aligned with objects in the physical model to accurately measure angles used to describe the position of various points in the model.

The first of these moving coordinate systems is aligned with the crossbars of the u-joint at B. The unit vector coordinate system is shown in *Figure 4.11* and is described by an orthogonal 3x3 matrix, **B**. The unit vector, $\boldsymbol{b_1}$, is oriented along the universal joint, U_4, yoke that connected to link 6 of the model. The unit vector, $\boldsymbol{b_2}$, is oriented along the universal joint, U_4, yoke that connected to the mobile platform of the model. The unit vector, $\boldsymbol{b_3}$, is orientated in a common right-hand coordinate system with respect to $\boldsymbol{b_1}$ and $\boldsymbol{b_2}$.

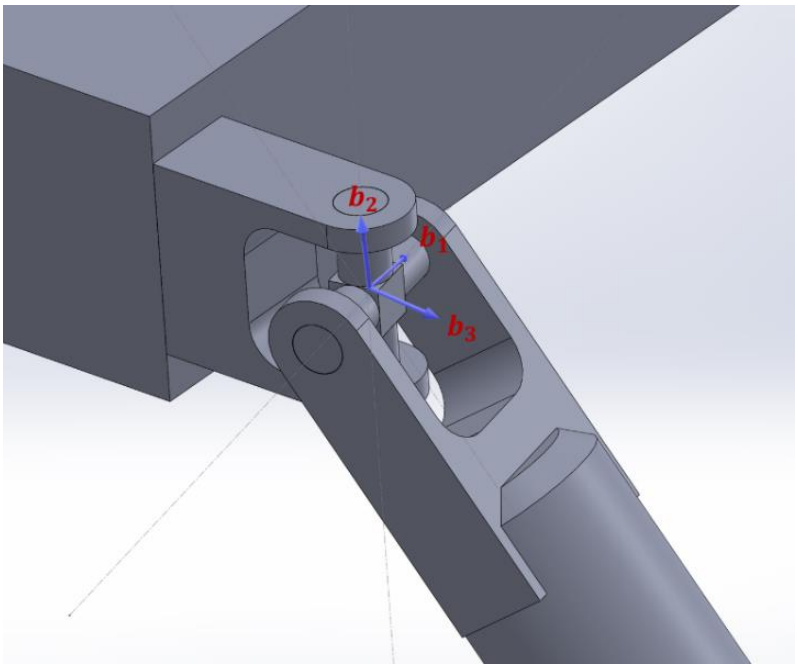

Figure 4.11: The B unit vector coordinate system

The first rotation is measured from negative $\hat{\jmath}$ axis to the $\boldsymbol{b_1}$ unit vector about the $\boldsymbol{b_3}$ unit vector or $\hat{\imath}$ axis by the angular displacement of θ_1. The second rotation is measured from the *YZ*-plane and about the displaced $\boldsymbol{b_1}$ unit vector by the angular displacement of θ_2. The third rotation is measured from $\boldsymbol{b_3}$ unit vector to the unit vector that follows the

line from point B to A about the displaced $\boldsymbol{b_2}$ unit vector by angular displacement of θ_3. The angle rotations are demonstrated in *Figure 4.12*.

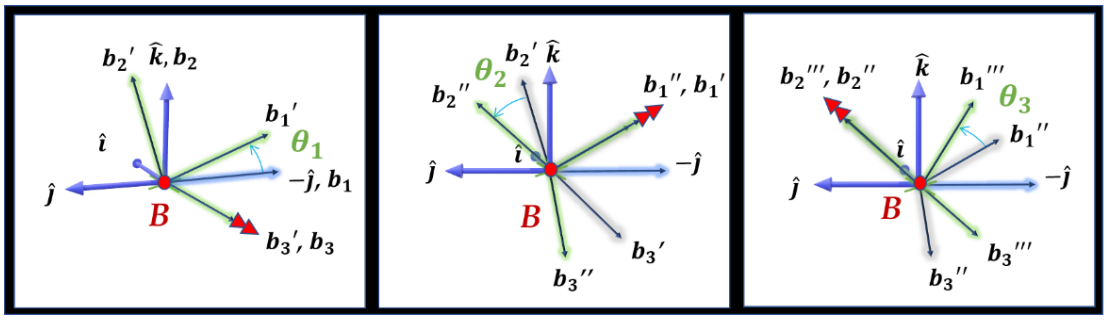

Figure 4.12: The measurement of $\boldsymbol{\theta_1, \theta_2,}$ and $\boldsymbol{\theta_3}$

The equation for the matrix **B** is expressed in *Equation 4.6.*

$$\boldsymbol{B}(\theta_1, \theta_2, \theta_3) = [\boldsymbol{b_1} \quad \boldsymbol{b_2} \quad \boldsymbol{b_3}] \tag{4.6}$$

Where

$$\boldsymbol{b_1} = \begin{bmatrix} \cos\theta_2 \sin\theta_3 \\ \sin\theta_1 \sin\theta_2 \sin\theta_3 - \cos\theta_1 \cos\theta_3 \\ \sin\theta_1 \cos\theta_3 + \cos\theta_1 \sin\theta_2 \sin\theta_3 \end{bmatrix}$$

$$\boldsymbol{b_2} = \begin{bmatrix} -\sin\theta_2 \\ \sin\theta_1 \cos\theta_2 \\ \cos\theta_1 \cos\theta_2 \end{bmatrix}$$

$$\boldsymbol{b_3} = \begin{bmatrix} -\cos\theta_2 \cos\theta_3 \\ -\cos\theta_1 \sin\theta_3 - \sin\theta_1 \sin\theta_2 \cos\theta_3 \\ \sin\theta_1 \sin\theta_3 - \cos\theta_1 \sin\theta_2 \cos\theta_3 \end{bmatrix}$$

The moving coordinate system at D can be described by an orthogonal 3x3 matrix, **D**. The unit vector coordinate system is shown in *Figure 4.13*. The unit vector, $\boldsymbol{d_1}$, is oriented along the universal joint, U_1, yoke that connected to prismatic joint, P_1, of the model. The unit vector, $\boldsymbol{d_2}$, is oriented along the universal joint, U_1, yoke that connected to link 4 of the model. The unit vector, $\boldsymbol{d_3}$, is orientated in a common right-hand coordinate system with respect to $\boldsymbol{d_1}$ and $\boldsymbol{d_2}$.

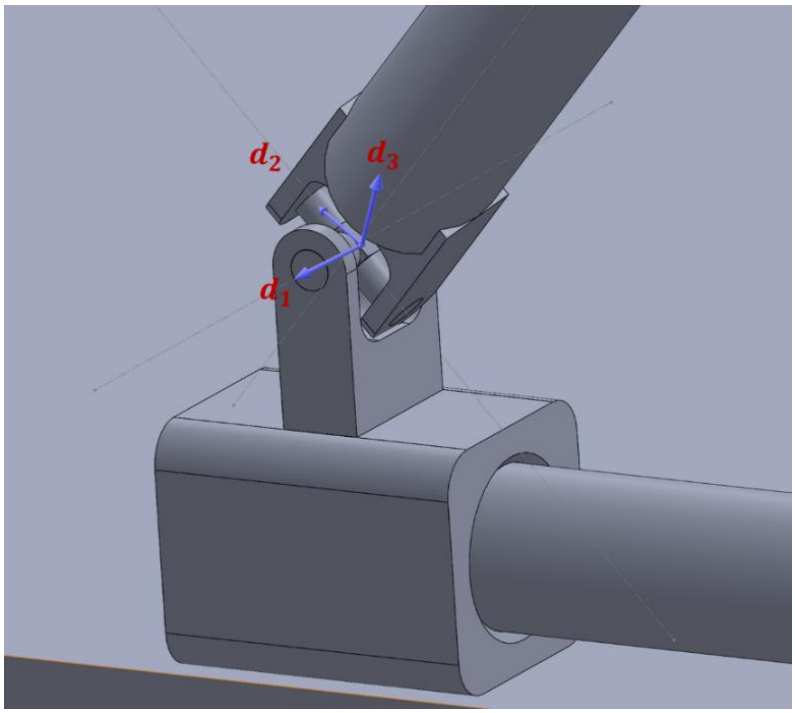

Figure 4.13: The D unit vector coordinate system

The ϕ_1 angle is measured from the negative $\hat{j}$ axis to the $\boldsymbol{d_2}$ unit vector about $\boldsymbol{d_1}$ unit vector. The ϕ_2 angle is measured from the $\boldsymbol{d_3}$ unit vector to link 4 about $\boldsymbol{d_2}$ unit vector. The measurement of these angles is shown in *Figure 4.14*.

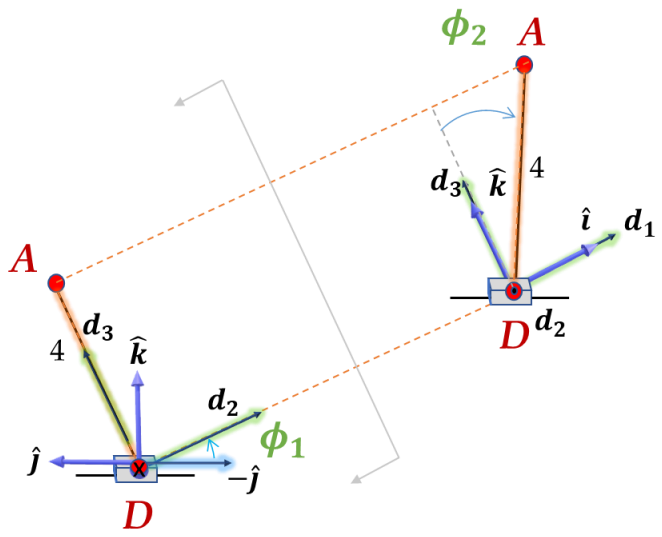

Figure 4.14: The measurement of ϕ_1 and ϕ_2, which has an orthographic projection from the ϕ_1 measurement

The equation for the matrix **D** is expressed in *Equation 4.7*.

$$\boldsymbol{D}(\phi_1, \phi_2) = [\boldsymbol{d_1} \quad \boldsymbol{d_2} \quad \boldsymbol{d_3}] \tag{4.7}$$

Where

$$\boldsymbol{d_1} = \begin{bmatrix} 1 \\ 0 \\ 0 \end{bmatrix}$$

$$\boldsymbol{d_2} = \begin{bmatrix} 0 \\ -\cos\phi_1 \\ \sin\phi_1 \end{bmatrix}$$

$$\boldsymbol{d_3} = \begin{bmatrix} 0 \\ \sin\phi_1 \\ \cos\phi_1 \end{bmatrix}$$

Finally, the moving coordinate system at E can be described by an orthogonal 3x3 matrix, **E**. The unit vector coordinate system is shown in *Figure 4.15*. The unit vector,

$\boldsymbol{e_1}$, is oriented along the universal joint, U_2, yoke that connected to prismatic joint, P_2, of the model. The unit vector, $\boldsymbol{e_2}$, is oriented along the universal joint, U_2, yoke that connected to link 4 of the model. The unit vector, $\boldsymbol{e_3}$, is orientated in a common right-hand coordinate system with respect to $\boldsymbol{e_1}$ and $\boldsymbol{e_2}$.

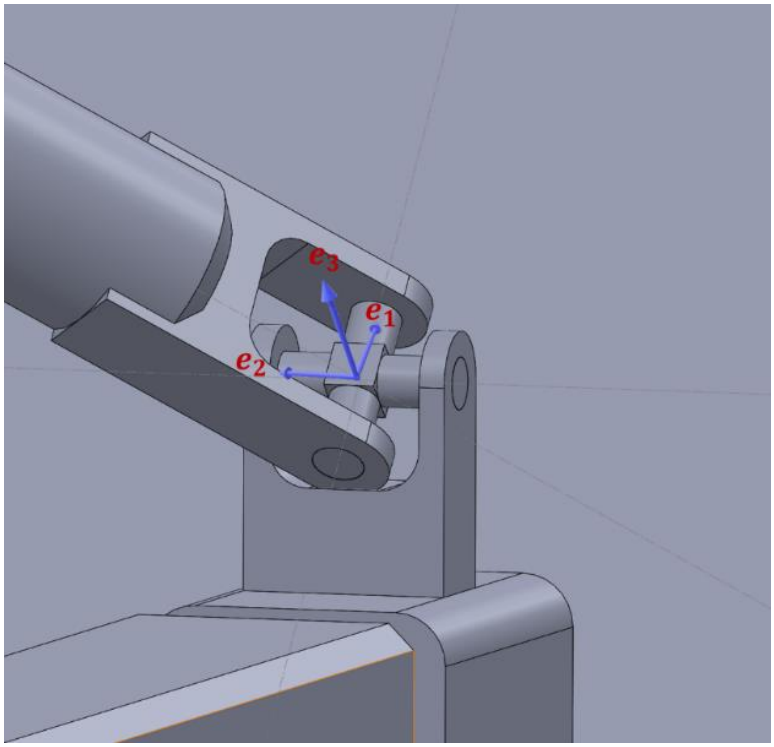

Figure 4.15: The E unit vector coordinate system

The θ_1 angle is measured from the negative $\hat{\jmath}$ axis to the $\boldsymbol{e_1}$ unit vector about $\boldsymbol{e_2}$ unit vector. This θ_1 angle is the same θ_1 angle from *Figure 4.12*. The $\boldsymbol{e_1}$ unit vector is parallel to $\boldsymbol{b_1}$ while $\boldsymbol{e_2}$ unit vector is parallel to the non-displaced $\boldsymbol{b_3}$ unit vector indicating that the two angle rotations are identical. The θ_4 angle is measured from the $\boldsymbol{e_3}$ unit vector to link 6 about $\boldsymbol{e_1}$ unit vector. The measurement of these angles is shown in *Figure 4.16*.

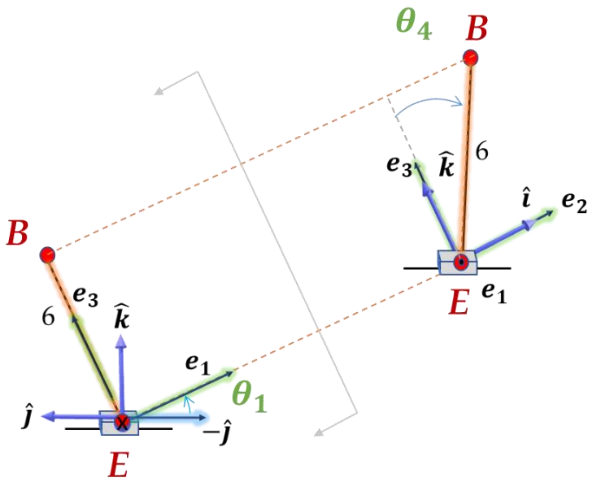

Figure 4.16: The measurement of θ_1 and θ_4, which has an orthographic projection from the θ_1 measurement

The equation for the matrix **E** is expressed in *Equation 4.8.*

$$\boldsymbol{E}(\theta_1, \theta_4) = [\boldsymbol{e_1} \quad \boldsymbol{e_2} \quad \boldsymbol{e_3}] \tag{4.8}$$

Where

$$\boldsymbol{e_1} = \begin{bmatrix} 0 \\ -\cos\theta_1 \\ \sin\theta_1 \end{bmatrix}$$

$$\boldsymbol{e_2} = \begin{bmatrix} 1 \\ 0 \\ 0 \end{bmatrix}$$

$$\boldsymbol{e_3} = \begin{bmatrix} 0 \\ \sin\theta_1 \\ \cos\theta_1 \end{bmatrix}$$

5. INVERSE KINEMATIC ANALYSIS

5.1 Solution overview

The objective of a solar tracker is to position the moving platform such that the surface of the moving platform is perpendicular to the sun's beam or direct radiation. This beam or direct radiation can be described using the position of sun vector **n**, or *Equation 4.1*. This means that the parallel manipulator output needs to correspond to the position of the sun vector. One way to find the inputs (i.e., the extension of the cylinders at D and E) required to orient the panel toward the sun's direct beam is to solve an inverse kinematic analysis.

The input for the 2-PUU/RS mechanism are the positions of the two prismatic slider joints, or P_1 and P_2. The corresponding output is the orientation of the mobile platform or the desired azimuth, γ, and elevation angles, α. The mobile platform of the parallel manipulator mechanism, where the solar panel is mounted, is connected to the base or ground through three kinematic chains. These three chains or legs as described earlier are an RS leg and two separate symmetrical PUU legs. These legs create two independent loops. A block diagram of the system solution is included in *Figure 5.1*.

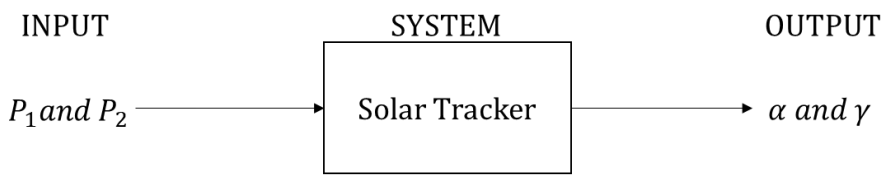

Figure 5.1: A block diagram of the solar tracker

The process to find the P_1 and P_2 dimensions that will create a desired orientation of the parallel manipulator begins with looking at the three loops created by the legs. The three loops can be described by vectors to and from different points located at the joints and corners of the mechanism. The three loops created by the legs can be defined as loops BEFC, ADFC, and ABED using the reference *Figure 4.7*. From these points, vector loop equations can be formed. Two of these loops are independent and can form loop closure equations that can be used to develop a system of scalar equations that can be used to analyze the position of the manipulator and solve the inverse kinematics problem.

`

5.2 Forming the loop closure equations

The kinematic analysis to find the input positions begins with choosing a set of loop closure equations to analyze. *Figure 5.2* highlights one loop closure equation, BEFC. BEFC is made up of one of the PUU legs and the RS leg.

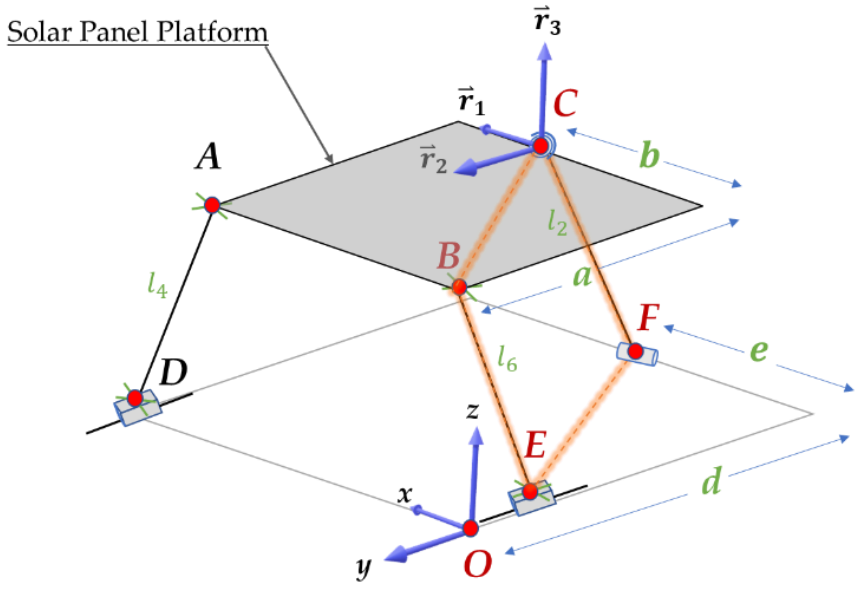

Figure 5.2: The BEFC loop

The parallel manipulator BEFC loop closure equation is described using two different expressions for the $\boldsymbol{R_{OC}}$ vector. This vector can be further broken into components from *Figure 5.2*. The first $\boldsymbol{R_{OC}}$ vector equation is shown in *Equation 5.1*.

$$\boldsymbol{R_{OC}} = \boldsymbol{R_{OE}} + \boldsymbol{R_{EB}} + \boldsymbol{R_{BC}} \tag{5.1}$$

The $\boldsymbol{R_{OE}}$ vector is simply from the origin, point O, to the position of the second prismatic joint in the *Y*-direction. The P_2 term is used to describe the second prismatic joint and the position of the second prismatic joint in relation to point O where the coordinate system resides. *Figure 5.3* shows the measurement of P_2 position based on the coordinate system residing at the corner.

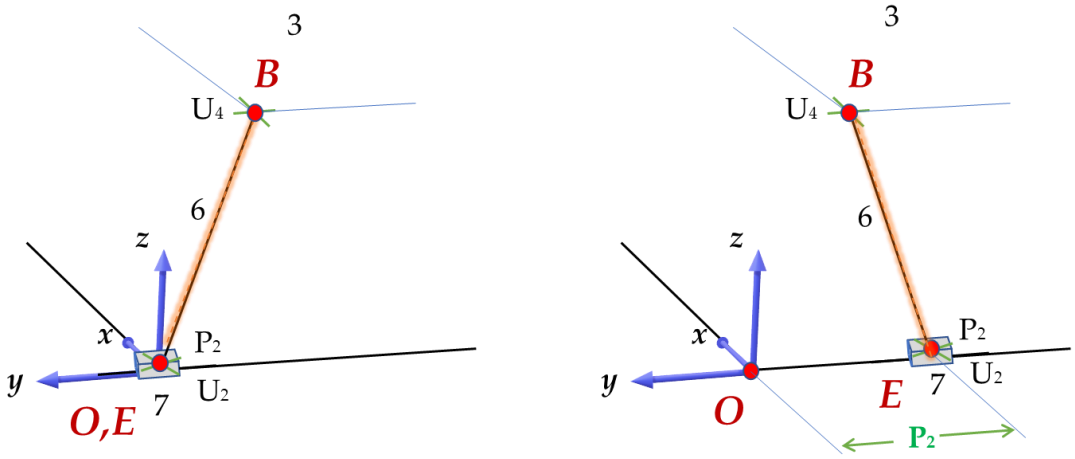

Figure 5.3: The measurement of P_2 (Left) starting position coincident with O, (Right) displaced position

$\boldsymbol{R_{OE}}$ is shown as *Equation 5.2*.

$$\boldsymbol{R_{OE}} = -P_2\hat{j} \tag{5.2}$$

The $\boldsymbol{R_{EB}}$ vector is made up of link 6 and its orientation. The l_6 term is the length of link 6. Link 6 is the intermediate member between the two universal joints, U_2 and U_4, labeled by points E and B. The θ_1 term is the angular rotation about the $\hat{\imath}$ unit vector axis measured from the negative $\hat{\jmath}$ unit vector axis. The θ_4 term is the angular rotation about $\hat{\jmath}$ unit vector axis measured from the e_3 unit vector, which is introduced in *Equation 4.8*. The angles θ_1 and θ_4 give the orientation of the vector. The θ_1 and θ_4 angle measurements are shown in *Figure 4.16*. $\boldsymbol{R_{EB}}$ is shown in *Equation 5.3*.

$$\boldsymbol{R_{EB}} = l_6[\,-\sin\theta_4,\ \cos\theta_4\sin\theta_1\,,\ \cos\theta_4\cos\theta_1]^{\mathrm{T}} \tag{5.3}$$

The $\boldsymbol{R_{BC}}$ vector goes from the universal joint, U_4, to the spherical joint, S_1, along with the mobile platform. The *a* and *b* dimensions define the length of the vector. The *a* dimension is the length of the mobile platform parallel to the *V*-axis. The *b* dimension is the midpoint of the length of the mobile platform parallel to the *U*-axis. The $\boldsymbol{r_1}$ and $\boldsymbol{r_2}$ unit vectors define the orientation along the mobile platform. The $\boldsymbol{r_1}$ and $\boldsymbol{r_2}$ are just two of the three mutually orthogonal the unit vectors from the rotation matrix defined for the coordinate system and described in *Equation 4.3*. The $\boldsymbol{R_{BC}}$ vector is shown in *Equation 5.4*.

$$\boldsymbol{R_{BC}} = b\boldsymbol{r_1} - a\boldsymbol{r_2} \tag{5.4}$$

The $\boldsymbol{R_{OC}}$ loop closure equation is completed using a second set of vectors to express $\boldsymbol{R_{OC}}$. The second $\boldsymbol{R_{OC}}$ vector equation is shown in *Equation 5.5*.

$$\boldsymbol{R_{OC}} = \boldsymbol{R_{OE}} + \boldsymbol{R_{EF}} + \boldsymbol{R_{FC}} \tag{5.5}$$

The $\boldsymbol{R_{OE}}$ vector is the same *Equation 5.2* from the first set. The $\boldsymbol{R_{EF}}$ vector from *Equation 5.5* starts from the prismatic joint, P_2, and continues to the revolute joint, R_1, along with the base of the tracker. The *d* and *e* terms define the length of the vector. The *d* dimension is the length of the base parallel to the *Y*-axis. The *e* dimension is the midpoint of the length of the base parallel to the *X*-axis. The base is defined by the position of prismatic joint sliders and revolute joint locations and is referred to as link 1. The $\boldsymbol{R_{EF}}$ vector relationship is defined in *Equation 5.6*.

$$\boldsymbol{R_{EF}} = e\hat{\boldsymbol{\imath}} + (P_2 - \mathrm{d})\hat{\boldsymbol{\jmath}} \tag{5.6}$$

The $\boldsymbol{R_{FC}}$ vector is defined by the length of link 2 and its orientation. The l_2 term is the length of link 2. Link 2 is the intermediate member between the revolute joint, R_1, and the spherical joint, S_1, labeled by points F and C. The β term is the angle of rotation about the *X*-axis measured from the $\hat{k}$ unit vector projected from the revolute joint, R_1. It defines the orientation of link 2. *Figure 5.4* shows the measurement of the β angle.

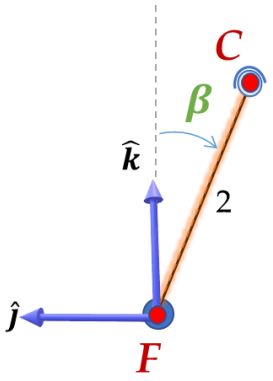

Figure 5.4: The β angle measurement [*X*-axis is going into the page]

The $\boldsymbol{R_{FC}}$ vector relationship is defined in *Equation 5.7*.

$$\boldsymbol{R_{FC}} = l_2[0,\ -\sin\beta,\ \cos\beta]^{\mathrm{T}} \tag{5.7}$$

The two equations, *Equation 5.1* and *Equation 5.5*, combine to create a loop closure equation, *Equation 5.8*.

$$\boldsymbol{R_{OE} + R_{EB} + R_{BC} - R_{OE} - R_{EF} - R_{FC} = 0} \tag{5.8}$$

The $\boldsymbol{R_{OE}}$ terms cancel each other out which leaves us with a modified *Equation 5.8*, which is shown as *Equation 5.9*. This provides three scalar equations in five unknowns: θ_1, θ_4, β, φ_3, and P_2.

$$\boldsymbol{R_{EB} + R_{BC} - R_{EF} - R_{FC} = 0} \tag{5.9}$$

The second loop closure equation can be constructed using the ADFC loop. *Figure 5.5* highlights the loop, ADFC. ADFC is made up of the other PUU leg and the same RS leg.

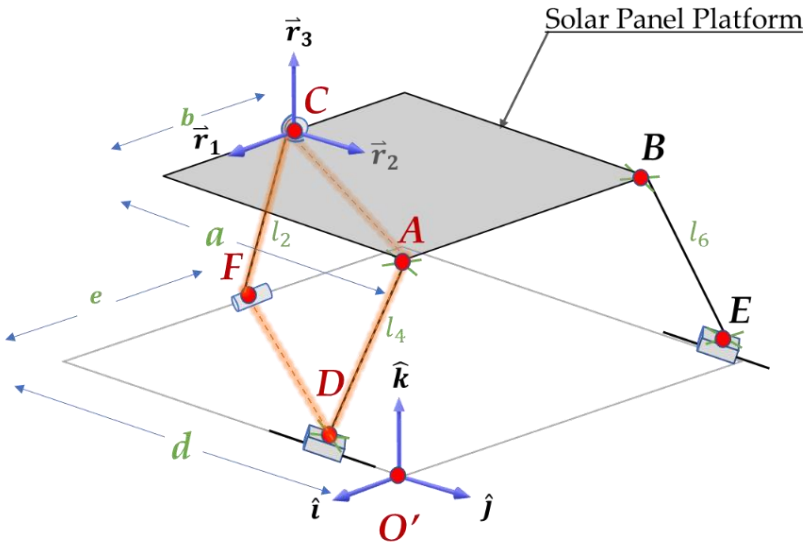

Figure 5.5: The ADFC loop

The parallel manipulator ADFC loop closure equation is described using the $\boldsymbol{R_{O'C}}$ vector. This vector can be further broken into components from *Figure 5.5*. The first $\boldsymbol{R_{O'C}}$ vector equation is shown in *Equation 5.10*.

$$\boldsymbol{R_{O'C} = R_{O'D} + R_{DA} + R_{AC}} \tag{5.10}$$

The $\boldsymbol{R_{O'D}}$ vector is simply from the reference origin, point O', to the position of the first prismatic joint in the *Y*-direction. The P_1 term is used to describe the first prismatic joint and the position of the first prismatic joint in relation to point O where the

coordinate system resides. The measurement of P_1 position is identical to the measurement of P_2 and shown in *Figure 5.6*.

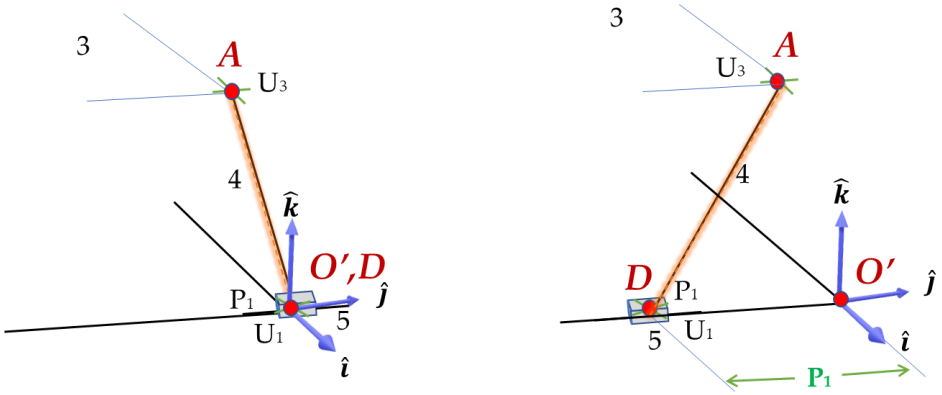

Figure 5.6: The measurement of P_1 (Left) starting position coincident with O', (Right) displaced position

$\boldsymbol{R_{O'D}}$ is shown as *Equation 5.11*.

$$\boldsymbol{R_{O'D}} = -P_1\hat{\jmath} \tag{5.11}$$

The $\boldsymbol{R_{DA}}$ vector is defined by link 4 and its orientation. The l_4 term is the length of link 4. Link 4 is the intermediate member between two points D and A which label the two universal joints, U_1 and U_3. The ϕ_1 term is the angular rotation about the $\hat{\imath}$ unit vector axis measured from the negative $\hat{\jmath}$ unit vector axis. The ϕ_2 term is the angular rotation about $\hat{\jmath}$ unit vector axis measured from the d_3 unit vector, which is introduced in *Equation 4.7*. The angles ϕ_1 and ϕ_2 describe the orientation of the vector. The ϕ_1 and ϕ_2 angle measurements are shown in *Figure 4.14*. $\boldsymbol{R_{DA}}$ is shown in *Equation 5.12*.

$$\boldsymbol{R_{DA}} = l_4[-\sin\phi_2,\ \cos\phi_2\sin\phi_1,\ \cos\phi_2\cos\phi_1]^{\mathrm{T}} \tag{5.12}$$

The $\boldsymbol{R_{AC}}$ vector goes from the universal joint, U_3, to the spherical joint, S_1, along with the mobile platform. The *a* dimension, *b* dimension, $\boldsymbol{r_1}$, and $\boldsymbol{r_2}$ are identical to the ones defined above for *Equation 5.4*. The $\boldsymbol{R_{AC}}$ vector is shown in *Equation 5.13*.

$$\boldsymbol{R_{BC}} = -b\boldsymbol{r_1} - a\boldsymbol{r_2} \tag{5.13}$$

The $\boldsymbol{R_{O'C}}$ loop closure equation is completed using another set of vectors which is equal to the first set. The second $\boldsymbol{R_{O'C}}$ vector equation is shown in *Equation 5.14*.

$$\boldsymbol{R_{O'C}} = \boldsymbol{R_{O'D}} + \boldsymbol{R_{DF}} + \boldsymbol{R_{FC}} \tag{5.14}$$

The $\boldsymbol{R_{O'D}}$ vector is the same as *Equation 5.11*. The $\boldsymbol{R_{DF}}$ vector from *Equation 5.14* starts from the prismatic joint, P_1, and continues to the revolute joint, R_1, along with the base of the parallel manipulator. The *d* and *e* terms are the same as the one defined above in *Equation 5.6*. The $\boldsymbol{R_{DF}}$ vector relationship is defined in *Equation 5.15*.

$$\boldsymbol{R_{DF}} = -e\hat{\boldsymbol{\imath}} + (P_1 - \mathrm{d})\hat{\boldsymbol{\jmath}} \tag{5.15}$$

The $\boldsymbol{R_{FC}}$ vector is defined the same as *Equation 5.7*. The two equations, *Equation 5.10* and *Equation 5.14*, combine to create a loop closure equation, *Equation 5.16*.

$$\boldsymbol{R_{O'D}} + \boldsymbol{R_{DA}} + \boldsymbol{R_{AC}} - \boldsymbol{R_{O'D}} - \boldsymbol{R_{DF}} - \boldsymbol{R_{FC}} = \boldsymbol{0} \tag{5.16}$$

The $\boldsymbol{R_{O'D}}$ terms cancel each other out which leaves us with a modified *Equation 5.16*. *Equation 5.17* shows the new equation. This provides three scalar equations with five unknowns: ϕ_1, ϕ_2, β, φ_3, and P_1.

$$\boldsymbol{R_{DA} + R_{AC} - R_{DF} - R_{FC} = 0} \tag{5.17}$$

Now, the combination of *Equation 5.9* and *Equation 5.17* provides a system of six scalar equation with eight unknowns. Accordingly, additional relationships created by the constraints of the mechanism must be identified.

5.3 Solving for parallel manipulator parameters

The loop closure equations create a system of six scalar equations with eight unknowns. This means that the system needs more equations or relationships to solve for the desired inputs. One such relationship can be found using the characteristics of the universal joint at point A. Point A has a universal joint, U_3, with two yokes, or cross members, that are perpendicular to each other. This is shown in *Figure 5.7*.

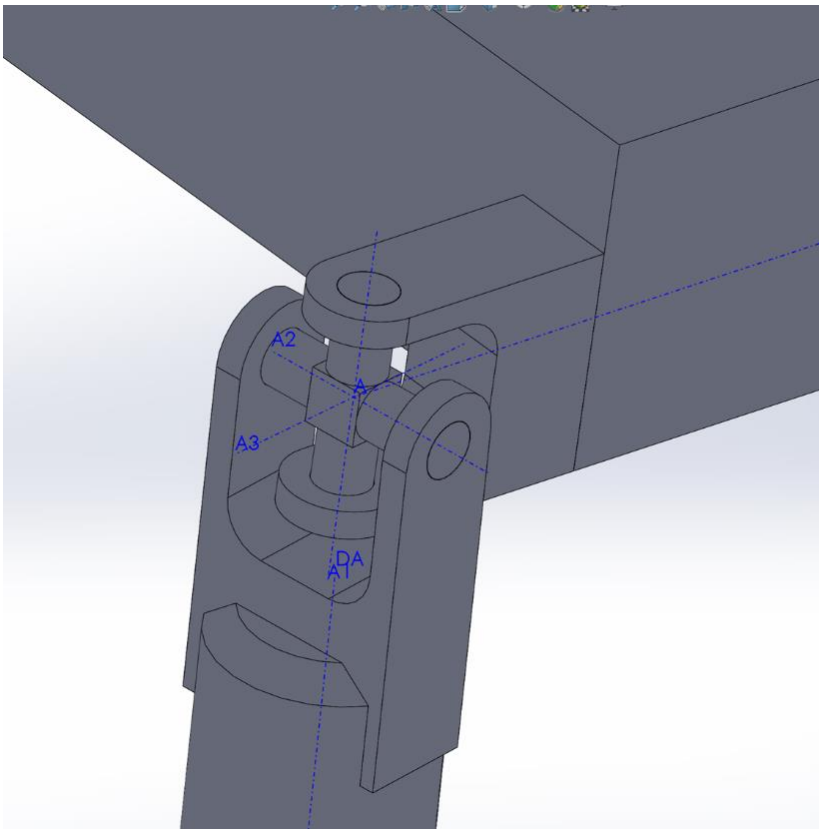

Figure 5.7: Point A on the parallel manipulator

One cross member is oriented with the mobile platform parallel to the moving *W*-axis. A similar cross member at point B is positioned parallel to this cross member and part of universal joint, U_4. This cross member has a pre-defined unit vector from *Equation 4.6* known as $\boldsymbol{b_2}$. The other cross member at point A is rigidly connected to the link 4. At the other end of link 4 is a parallel cross member at point D. This cross member is a part of the universal joint, U_1, and has a pre-defined unit vector from *Equation 4.7* known as $\boldsymbol{d_2}$. The dot product of two perpendicular unit vectors is zero. Therefore, by using the two unit vectors $\boldsymbol{b_2}$ and $\boldsymbol{d_2}$, an equation can be formed. This is *Equation 5.18*.

$$\boldsymbol{b_2} \cdot \boldsymbol{d_2} = \mathbf{0} \tag{5.18}$$

Where

$$\boldsymbol{b_2} = -\sin\theta_2\,\hat{\boldsymbol{\imath}} + \cos\theta_2 \sin\theta_1\,\hat{\boldsymbol{\jmath}} + \cos\theta_2 \cos\theta_1\,\hat{\boldsymbol{k}}$$

$$\boldsymbol{d_2} = 0\hat{\boldsymbol{\imath}} - \cos\phi_1\,\hat{\boldsymbol{\jmath}} + \sin\phi_1\,\hat{\boldsymbol{k}}$$

Using *Equation 5.18,* a new relationship between ϕ_1, θ_1, and θ_2 is formed in *Equation 5.19*.

$$(\cos\theta_2 \sin\theta_1)(-\cos\phi_1) + (\cos\theta_2 \cos\theta_1)(\sin\phi_1) = 0 \tag{5.19}$$

Equation 5.19 can then be rearranged to find the relationship in *Equation 5.20*.

$$\tan\theta_1 = \tan\phi_1 \tag{5.20}$$

Equation 5.20 reveals that θ_1 and ϕ_1 are equal or 180˚ apart; however, for this parallel manipulator special case, they are assumed to be equal because it is consistent with the manipulator that was modeled. Therefore, θ_1 and $\phi_1$in these equations are going to be defined as equal, thus eliminating one of the eight unknowns, giving just seven unknowns.

While *Equation 5.20* eliminates one extra unknown, there are still seven unknowns with a system of only six scalar equations. Another relationship can be formed to eliminate this final extra unknown. As discussed before, the $\boldsymbol{b_2}$ unit vector is parallel to the moving *W*-axis of the mobile platform. The orientation of the *W*-axis of the mobile platform can be described by the unit vector $\boldsymbol{r_3}$. Therefore, the two unit vectors $\boldsymbol{b_2}$ and $\boldsymbol{r_3}$ are parallel and equal to each other. This relationship is defined in *Equation 5.21*.

$$\boldsymbol{b_2} = \boldsymbol{r_3} \tag{5.21}$$

Where

$$\boldsymbol{b_2} = \begin{bmatrix} -\sin\theta_2 \\ \sin\theta_1\cos\theta_2 \\ \cos\theta_1\cos\theta_2 \end{bmatrix}$$

$$\boldsymbol{r_3} = \begin{bmatrix} \sin\varphi_2\sin\varphi_1 \\ -\sin\varphi_2\cos\varphi_1 \\ \cos\varphi_2 \end{bmatrix}$$

Using *Equation 5.21*, three scalar equations are created and shown as *Equation 5.22*, *Equation 5.23,* and *Equation 5.24*.

$$-\sin\theta_2 - \sin\varphi_2\sin\varphi_1 = 0 \tag{5.22}$$

$$\sin\theta_1\cos\theta_2 + \sin\varphi_2\cos\varphi_1 = 0 \tag{5.23}$$

$$\cos\theta_1\cos\theta_2 - \cos\varphi_2 = 0 \tag{5.24}$$

These equations can then be used to find an expression to solve for the two unknowns, $\theta_1$and θ_2. *Equation 5.25*, *Equation 5.26*, *Equation 5.27*, and *Equation 5.28* display the relationship with γ and α substituted in for φ_1 and φ_2.

$$\theta_2 = \sin^{-1}(-\sin\gamma\sin(\alpha - 90°)) \tag{5.25}$$

$$\sin\theta_1 = \frac{-\cos\gamma\sin(\alpha - 90°)}{\cos\theta_2} \tag{5.26}$$

$$\cos\theta_1 = \frac{\cos(\alpha - 90°)}{\cos\theta_2} \tag{5.27}$$

Where

$$\theta_1 = \arctan2(\sin\theta_1, \cos\theta_1) \tag{5.28}$$

This relationship can be applied to the system of equations created by *Equation 5.9* and *Equation 5.17*, resulting in a system of eight scalar equations in eight unknowns. The eight scalar equations are listed as *Equation 5.29* through *Equation 5.36*.

$$-e - l_6\sin\theta_4 + a[\cos\gamma\sin\varphi_3 - \sin\gamma\cos(\alpha - 90°)\cos\varphi_3] + b[\cos\gamma\cos\varphi_3 + \sin\gamma\cos(\alpha - 90°)\sin\varphi_3] = 0 \tag{5.29}$$

$$d - P_2 + l_2\sin\beta + l_6\cos\theta_4\sin\theta_1 - a[\sin\gamma\sin\varphi_3 + \cos\gamma\cos\varphi_3\cos(\alpha - 90°)] - b[\sin\gamma\cos\varphi_3 - \cos\gamma\cos(\alpha - 90°)\sin\varphi_3] = 0 \tag{5.30}$$

$$l_6\cos\theta_4\cos\theta_1 - l_2\cos\beta - a[\sin(\alpha - 90°)\cos\varphi_3] + b[\sin(\alpha - 90°)\sin\varphi_3] = 0 \tag{5.31}$$

$$e - l_4\sin\phi_2 + a[\cos\gamma\sin\varphi_3 - \sin\gamma\cos(\alpha - 90°)\cos\varphi_3] - b[\cos\gamma\cos\varphi_3 + \sin\gamma\cos(\alpha - 90°)\sin\varphi_3] = 0 \tag{5.32}$$

$$d - P_1 + l_2\sin\beta + l_4\cos\phi_2\sin\theta_1 - a[\sin\gamma\sin\varphi_3 + \cos\gamma\cos(\alpha - 90°)\cos\varphi_3] + b[\sin\gamma\cos\varphi_3 - \cos\gamma\cos(\alpha - 90°)\sin\varphi_3] = 0 \tag{5.33}$$

$$l_4\cos\theta_1\cos\phi_2 - l_2\cos\beta - a[\sin(\alpha - 90°)\cos\varphi_3] - b[\sin(\alpha - 90°)\sin\varphi_3] = 0 \quad (5.34)$$

$$\theta_2 = \sin^{-1}(-\sin\gamma\sin(\alpha - 90°)) \quad (5.35)$$

$$\theta_1 = \arctan2\left(\frac{-\cos\gamma\sin(\alpha - 90°)}{\cos\theta_2}, \frac{\cos(\alpha - 90°)}{\cos\theta_2}\right) \quad (5.36)$$

The eight unknowns are ϕ_2, θ_1, θ_2, θ_4, β, φ_3, P_1, and P_2.

6. RESULTS

After an analysis of the mechanism, a system of scalar equations has been found to solve the inverse kinematics problem. Using numerical solver in MATLAB, see *Appendix A* and *Appendix B* for the code, one solution to the set of scalar equations is provided below for an arbitrary set of manipulator parameters. The goal was to provide a mechanism to achieve various azimuth and elevation angles throughout the day to track the sun. A SolidWorks model is used to validate the results and display the various positions. This solution shows the parallel manipulator can achieve a range of azimuth and elevation angles. The parameters for this specific solar tracker are displayed in *Table 6.1*.

Table 6.1: The parameters for an example parallel manipulator solar tracker

Parameter	Description	Specification [inches]
a	Length of mobile platform	76
b	Midpoint width of mobile platform	38
d	Length of the base	71.5
e	Midpoint width of base	38
l_2	Length of Link 2	74.5
l_4	Length of Link 4	36
l_6	Length of Link 6	36

This solution can reach a range of positions depending on the specification of the inputs, P_1 and P_2. The first example position displayed is where both P_1 and P_2 are in the retracted position where they align with point O and are equal. The variables are displayed in *Table 6.2* for example position 1. Example position 1 is displayed in *Figure 6.1*.

Table 6.2: The variables for example position 1 for solar tracker

Parameter	Description	Specification
γ	Azimuth Angle	0^o
α	Elevation Angle	58.8^o
P_1	Prismatic Joint 1 Extension Length	0 inches
P_2	Prismatic Joint 2 Extension Length	0 inches
θ_1	The angular rotation about $\boldsymbol{b_3}$unit vector	31.2^o
θ_2	The angular rotation about $\boldsymbol{b_1}$unit vector	0^o
θ_3	The angular rotation about $\boldsymbol{b_2}$unit vector	0^o
θ_4	The angular rotation about $\boldsymbol{e_1}$unit vector	0^o
ϕ_1	The angular rotation about $\boldsymbol{d_1}$unit vector	31.2^o
ϕ_2	The angular rotation about $\boldsymbol{d_2}$unit vector	0^o
β	The angular rotation about revolute joint at C	-19.6^o

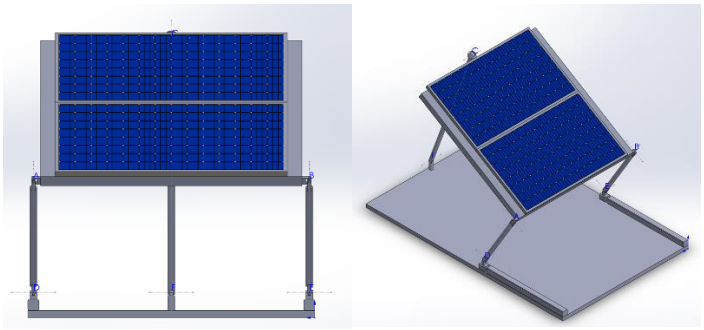

Figure 6.1: The parallel manipulator solar tracker in example position 1 [$\gamma = 0^o$ and $\alpha = 58.8^o$]

The second example position demonstrated is where P_1 is extended fully and P_2 remains retracted to where it aligns with point O. The variables are displayed in *Table 6.3* for example position 2. Example position 2 is displayed in *Figure 6.2*.

Table 6.3: The variables for example position 2 for solar tracker

Parameter	Description	Specification
γ	Azimuth Angle	22.2º
α	Elevation Angle	38.8º
P_1	Prismatic Joint 1 Extension Length	47 inches
P_2	Prismatic Joint 2 Extension Length	0 inches
θ_1	The angular rotation about $\boldsymbol{b_3}$unit vector	49.1º
θ_2	The angular rotation about $\boldsymbol{b_1}$unit vector	-17.1º
θ_3	The angular rotation about $\boldsymbol{b_2}$unit vector	-23.9º
θ_4	The angular rotation about $\boldsymbol{e_1}$unit vector	-71.9º
ϕ_1	The angular rotation about $\boldsymbol{d_1}$unit vector	49.1º
ϕ_2	The angular rotation about $\boldsymbol{d_2}$unit vector	-43.2º
β	The angular rotation about revolute joint at C	-18.4º

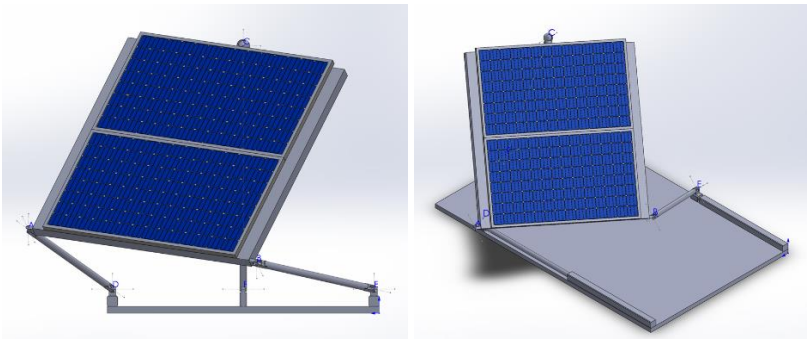

Figure 6.2: The parallel manipulator solar tracker in example position 2, which has P_1 fully extended and P_2 is retracted [γ = 22.2º and α = 38.8º]

The third example position demonstrated is where P_2 is extended fully and P_1 becomes retracted to where it aligns with point O. The variables are displayed in *Table 6.4* for example position 3. Example position 3 is displayed in *Figure 6.3*.

Table 6.4: The variables for example position 3 for solar tracker

Parameter	Description	Specification
γ	Azimuth Angle	-22.2º
α	Elevation Angle	38.8º
P_1	Prismatic Joint 1 Extension Length	0 inches
P_2	Prismatic Joint 2 Extension Length	47 inches
θ_1	The angular rotation about $\boldsymbol{b_3}$ unit vector	49.1º
θ_2	The angular rotation about $\boldsymbol{b_1}$ unit vector	17.1º
θ_3	The angular rotation about $\boldsymbol{b_2}$ unit vector	23.9º
θ_4	The angular rotation about $\boldsymbol{e_1}$ unit vector	43.2º
ϕ_1	The angular rotation about $\boldsymbol{d_1}$ unit vector	49.1º
ϕ_2	The angular rotation about $\boldsymbol{d_2}$ unit vector	71.9º
β	The angular rotation about revolute joint at C	-18.4º

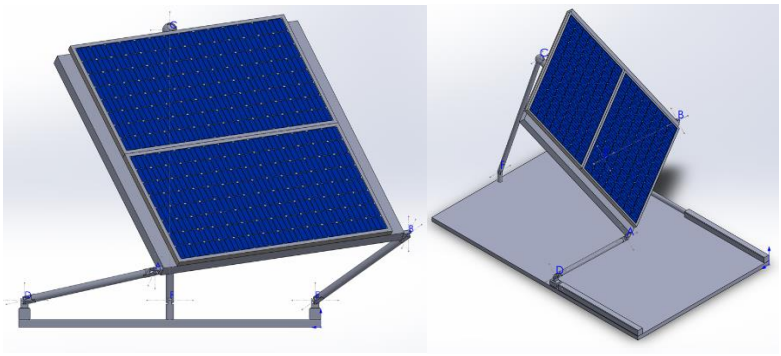

Figure 6.3: The parallel manipulator solar tracker in example position 3, which has P_2 fully extended and P_1 is retracted [γ = -22.2º and α = 38.8º]

The mechanism can reach a range of other azimuth and elevation angles besides the three example positions demonstrated. For these dimensions, *Figure 6.4* shows the azimuth and elevation angles possible are overlaid on the sun path for March 21st, 2019. March 21st, 2019 is the day after the solar equinox.

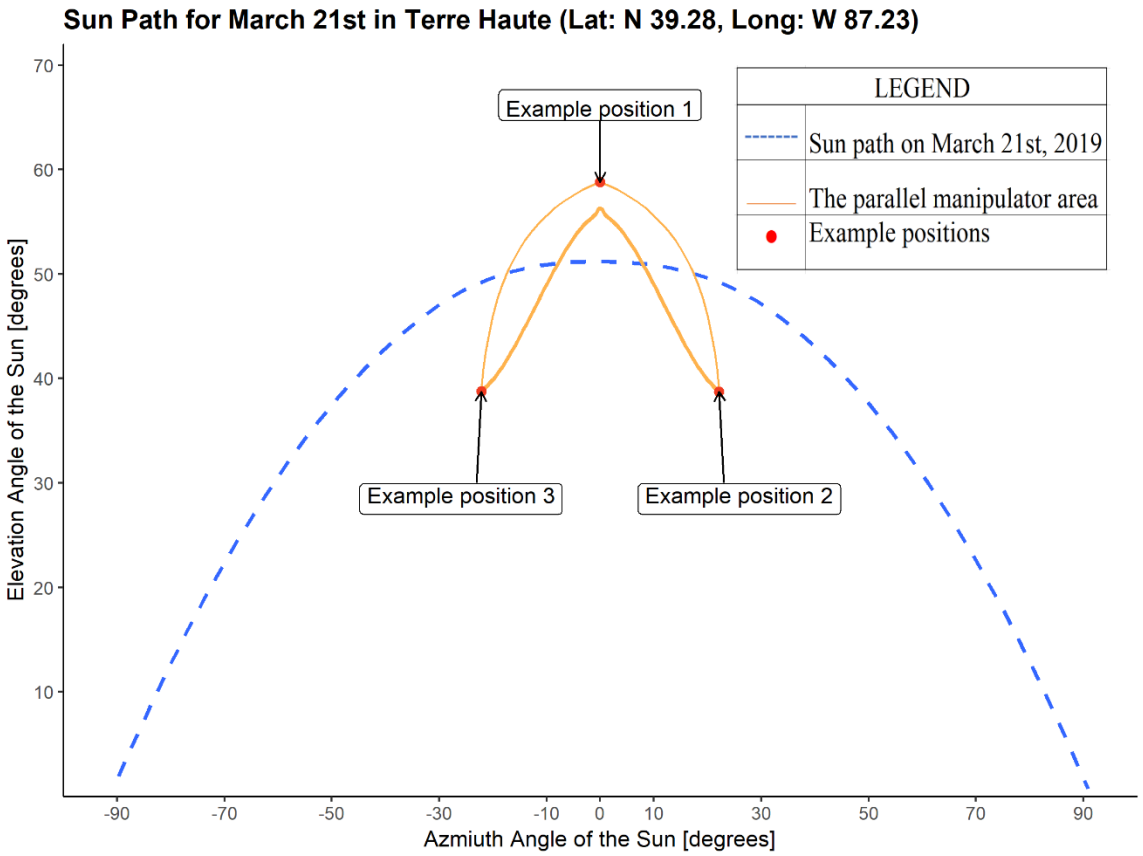

Figure 6.4: The possible azimuth and elevation angles for the solar tracker overlaid on the path of the sun on March 21st, 2019

7. LIMITATIONS

The parameters for the example solar tracker presented in the results section were selected arbitrarily and do not optimize the workspace of the manipulator for solar tracking. As *Figure 6.6* shows, it only encompasses a portion of the sun's path. The plot in *Figure 6.6* also only shows one day of the year and the path of the sun changes throughout the year due to the rotations of the earth. The ideal solar tracker has a workspace that encompasses the path of the sun throughout most of each day throughout the year - which is not the case for the example solar tracker.

While the parameters of the presented example manipulator have not been optimized for matching the manipulator's workspace to the path of the sun, there are other factors that may also artificially limit the size and shape of the workspace. These limitations are due to a few reasons. First, the inverse kinematics analysis was developed for a special case in which the joints and links were limited to certain orientations and planes. For example, the inverse kinematics model is based on the prismatic joints aligning parallel to the *Y*-axis. This doesn't have to be the case and the prismatic joints can be placed at an angle or not be symmetrical at all. This may prove to be a better configuration but was not explored. Another possible limitation was forcing A, B, and C into the same *UV*-plane. Alternative workspaces could be achieved by tilting the mobile platform so that C is placed out of the *UV*-plane. This could allow for a larger change in elevation angle without increasing the length of any of the links. It may also allow for a larger range in azimuth angles than is displayed by the example manipulator that was presented.

Essentially, creating a more general model could lead to a better configuration to increase the workspace.

8. FUTURE WORK

This thesis explores creating a novel solar tracking using a parallel manipulator. Although the device presented can achieve changing azimuth and elevation angles to try and map to the sun's path, it may not be the most optimal configuration. A more general model of the 2-PUU/RS parallel manipulator can be developed. This could lead to more optimal joint and link placement in different planes or parallel to certain axes like the ideas discussed in the limitations section.

The model parameters were also not optimal for the special case used. Optimization of parameters can increase the azimuth and elevation angles that are reachable by the manipulator. Workspace optimization is an important step to the design process. Workspace optimization finds the parameters that allow it to match the path of the sun as closely as possible. It also can create a well-conditioned workspace to provide no toggle positions or reduce large output errors.

Ultimately, this is only the first step toward creating solar trackers using parallel manipulators. There is more work to be done, but the parallel manipulator model has proven to be able to track the sun through a portion of its path. Hopefully, this thesis will serve as one of the stepping stones that may allow parallel manipulators to be the future of solar tracking.

LIST OF REFERENCES

[1] Schmela, Michael. "Global Market Outlook 2018-2022." SolarPower Europe. June 27, 2018. Accessed December 12, 2018. http://www.solarpowereurope.org/global-market-outlook-2018-2022/.

[2] "Key World Energy Statistics 2018." Key World Energy Statistics, 2018, 14. Accessed December 11, 2018. doi:10.1787/key_energ_stat-2018-en.

[3] Tibbits, Thomas N. D., *et al*. "Wafer Bonded Four-junction GaInP/GaAs//GaInAsP/GaInAs Concentrator Solar Cells with 44.7% Efficiency." Progress in Photovoltaics: Research and Applications 22, no. 3 (2014): 277-82. Accessed December 11, 2018. doi:10.1002/pip.2475.

[4] Aggarwal, Vikram. "Solar Panel Efficiency: What Panels Are Most Efficient? | EnergySage." Solar News. December 03, 2018. Accessed December 12, 2018. https://news.energysage.com/what-are-the-most-efficient-solar-panels-on-the-market/.

[5] "Research Cell Efficiency Records." Department of Energy. September 2015. Accessed February 01, 2019. https://www.energy.gov/eere/solar/downloads/research-cell-efficiency-records.

[6] Finster, Curt. "El Heliostato De La Universidad Santa Maria." Scientia 119 (1962): 5-20.

[7] Barak, Amitzur. Turning Collectors for Solar Radiation. US Patent 3,982,526, filed March 20, 1975, and issued September 28, 1976.

[8] Brantley, Lott W., and Billy D. Lawson. Mount for Continuously Orientating a Collector Dish In a System Adapted to Perform Both Diurnal and Seasonal Solar Tracking. US Patent 4,011,854, filed January 29, 1976, and issued March 15, 1977.

[9] Gay, C.F., Wilson, J.H., and Yerkes, J.W. Wed. "Performance advantages of two-axis tracking for large flat-plate photovoltaic energy systems". United States.

[10] Mohammad, Nur, and Tarequl Karim. "Design and Implementation of Hybrid Automatic Solar-Tracking System." Journal of Solar Energy Engineering 135, no. 1 (2012): 011013. Accessed December 11, 2018. doi:10.1115/1.4007295.

[11] Corio, Ronald P. Single-Axis Solar Tracking System. US Patent 8,459,249, filed June 12, 2008, and issued June 11, 2013.

[12] Corio, Ronald P. Single-Axis Solar Tracking System. US Patent 9,631,840, filed May 15, 2013, and issued April 25, 2017.

[13] Au, Alexander W. Frameless Solar Module Mounting. US Patent 9,543,888, filed June 9, 2015, and issued January 10, 2017.

[14] Au, Alexander W. Horizontal Balanced Solar Tracker. US Patent 9,905,717, filed December 9, 2013, and issued February 27, 2018.

[15] Au, Alex, and Yang Liu. Self-Powered Solar Tracker Apparatus. US Patent 10,075,125, filed December 16, 2015, and issued September 11, 2018.

[16] Meydbray, Yevgeny. Variable Tilt Tracker for Photovoltaic Arrays. US Patent 8,776,781, filed July 30, 2008, and issued July 15, 2014.

[17] Lamoureux, Aaron, *et al*. "Dynamic Kirigami Structures for Integrated Solar Tracking." Nature Communications 6, no. 1 (2015). Accessed December 11, 2018. doi:10.1038/ncomms9092.

[18] Huang, B.j., and F.s. Sun. "Feasibility Study of One Axis Three Positions Tracking Solar PV with Low Concentration Ratio Reflector." Energy Conversion and Management 48, no. 4 (2007): 1273-280. Accessed December 11, 2018. doi:10.1016/j.enconman.2006.09.020.

[19] Sherman, James. Solar Tracking System. US Patent 8,946,608, filed August 19, 2013, and issued February 3, 2015.

[20] Amin, Nowshad, Mohammad Rezaul Karim, Mamdooh S. Al-Saud, and Abdulrahman M. Al-Ahmari. Dual Axis Solar Tracking Apparatus and Method. US Patent 8,895,836, filed October 19, 2011, and issued November 25, 2014.

[21] Jeng, Shyr-Long, Bin-Han Lue, and Wei-Hua Chieng. "Design and Analysis of Spatial Parallel Manipulator for Dual Axis Solar Tracking." Journal of Chinese Society of Mechanical Engineering 35, no. 3 (2014): 221-31. Retrieved December 4, 2018.

[22] Trujillo, Saloman J., Vayardo L. Ruiz, Noe Esparza, Jessica A. Riley, Kevin C. Chu, and Wasiq Bokhari. Solar Tracking System Employing Multiple Mobile Robots. US Patent 9,494,341, filed September 10, 2013, and issued November 15, 2016.

[23] Pandilov, Zoran, and Vladimir Duk. "Comparison of the Characteristics Between Serial and Parallel Robots." ACTA TEHNICA CORVINIENSIS – Bulletin of Engineering Tome VII, no. Fascicule 1 (2014): 143-60. Accessed December 11, 2018.

[24] Tsai, Lung-Wen. Mechanism Design: Enumeration of Kinematic Structures According to Function. Boca Raton: CRC Press, 2001.

APPENDICES

APPENDIX A

Appendix A shows a commented Matlab file that was used to solve the system of equations

```
%%%%%%%%%%%%%%%%%%%%%%%%%%%%%%%%%%%%%%%%%%%%%%%%%%%%%%%%%%%%%%%%%%%%%%%%%%%%%%%%
% Author: Joseph Hubach
% Date:   2019 February 02
% Description: Solve System of equations to find the variables of the
%              Parallel manipulator solar tracker
%%%%%%%%%%%%%%%%%%%%%%%%%%%%%%%%%%%%%%%%%%%%%%%%%%%%%%%%%%%%%%%%%%%%%%%%%%%%%%%%
clc
clear variables
%%%%%%%%%%%%%%%%%%%%%%%%%%%%%%%%%%%%%%%%%%%%%%%%%%%%%%%%%%%%%%%%%%%%%%%%%%%%%%%%
%  define the function that is being solved
fun = @Solve_Parallel_Manipulator_System_of_Equations;

%  Set Intial Guesses for unknowns
x0 = [5,5,5,5,20,0];

% The options for fsolve fucntion
options = optimoptions('fsolve');
options.MaxIterations = 1000000;
options.MaxFunctionEvaluations = 1000000;

% Execute fsolve to solve for unknowns
x = fsolve(fun,x0,options)
```

APPENDIX B

Appendix B shows a commented Matlab function file that was used in Appendix A to solve the system of equations

```
function F=Solve_Parallel_Manipulator_System_of_Equations(x)
% Function File to Solve System of Equations for Parallel Manipulator
% Author: Joseph Hubach
% Date:   2019 February 02


% Assigning the parameters for the Parallel Manipulator
% Mobile Platform Dimensions [inches]
a = 76;
b = 76/2;

% An extra mobile platform parameter if C is out of the UV-plane
c = 0;

% Base Dimensions [inches]
d = 71.5;
e = 76/2;

% Link Lengths [inches]
l4 = 36;
l6 = 36;
l2 = 74.5;

% Define Azimuth and Elevation Angles [degrees]
el = 47.5953;
az = -19.1446;

% Assign angles p1 and p2 in terms of Azimuth and Elevation [degrees]
p1 = -az;
p2 = el-90;

%  Defining the unknown values
%  *(only 6 equations and 6 unknowns will be solved using fsolve function)
phi2   = x(1);
theta4 = x(2);
beta   = x(3);
p3     = x(4);
```

```
P1     = x(5);
P2     = x(6);


%  Defining two of the unknown values (theta1 and theta2)
%  using B2 = R3 vectors

% Equation 5.35
theta2 = asind(-sind(-az)*sind(el-90));
% Equation 5.26
sint1  = -cosd(az)*sind(el-90)/cosd(theta2);
% Equation 5.27
cost1  = cosd(el-90)/cosd(theta2);
% Equation 5.36
theta1 = atan2(sint1,cost1)*180/pi;

% The relationship from tan(phi1) = tan (theta1)

% Equation 5.20
phi1 = theta1;

%  Defining the system of equations (Equations 5.29 through 5.34)

% Equation 5.29
F(1) = a*(cosd(p1)*sind(p3) + cosd(p2)*cosd(p3)*sind(p1)) - 1.0*e +
b*(cosd(p1)*cosd(p3) - 1.0*cosd(p2)*sind(p1)*sind(p3)) - 1.0*l6*sind(theta4) -
1.0*c*sind(p1)*sind(p2);
% Equation 5.30
F(2) = d - 1.0*P2 + b*(cosd(p3)*sind(p1) + cosd(p1)*cosd(p2)*sind(p3)) +
a*(sind(p1)*sind(p3) - 1.0*cosd(p1)*cosd(p2)*cosd(p3)) + l2*sind(beta) +
c*cosd(p1)*sind(p2) + l6*cosd(theta4)*sind(theta1);
% Equation 5.31
F(3) = l6*cosd(theta1)*cosd(theta4) - 1.0*c*cosd(p2) - 1.0*a*cosd(p3)*sind(p2) -
1.0*l2*cosd(beta) + b*sind(p2)*sind(p3);
% Equation 5.32
F(4) = e + a*(cosd(p1)*sind(p3) + cosd(p2)*cosd(p3)*sind(p1)) -
1.0*b*(cosd(p1)*cosd(p3) - 1.0*cosd(p2)*sind(p1)*sind(p3)) - 1.0*l4*sind(phi2) -
1.0*c*sind(p1)*sind(p2);
% Equation 5.33
F(5) = d - 1.0*P1 - 1.0*b*(cosd(p3)*sind(p1) + cosd(p1)*cosd(p2)*sind(p3)) +
a*(sind(p1)*sind(p3) - 1.0*cosd(p1)*cosd(p2)*cosd(p3)) + l2*sind(beta) +
c*cosd(p1)*sind(p2) + l4*cosd(phi2)*sind(phi1);
% Equation 5.34
F(6) = l4*cosd(phi1)*cosd(phi2) - 1.0*c*cosd(p2) - 1.0*l2*cosd(beta) -
1.0*a*cosd(p3)*sind(p2) - 1.0*b*sind(p2)*sind(p3);
end
```